APPLICATION OF A CALIBRATED AEROSOL CAVITY RING DOWN SPECTROMETER AT 355 NM FOR THE MEASUREMENT OF SCATTERING AND ABSORBING HOMOGENEOUS AEROSOLS AND AEROSOL MIXTURES

by

KIMBERLY J SCHULDT

(Under the Direction of Geoffrey Smith)

ABSTRACT

The interaction of aerosol particles and solar radiation plays an important role in the global radiative balance. Discussed in this work is the use of cavity ring down spectroscopy for the measurement of complex refractive indices for homogeneous aerosols and aerosol mixtures. Application of a novel calibration method improved the uncertainty of extinction cross section measurements collected from 10.6% to 2%. This technique retrieved complex refractive index measurements in close agreement with the values predicted by the volume-fraction mixing rule for an absorbing binary mixture composed of 2-(2-benzotriazol-2-yl)-6-dodecyl-4-methylphenol (BDMP), a strong UV absorber, and squalane. These measurements demonstrate high sensitivity and the ability to measure atmospherically relevant absorption. Measurements of aerosol external mixtures demonstrated the ability to measure the contribution of multiple-charged particles to measured extinction cross sections at small particle diameters. An initial investigation into the importance of phase in aerosol optical properties is also described.

INDEX WORDS: cavity ring down spectroscopy; complex refractive index; aerosol; optical properties; UV; volume fraction mixing rule; internal mixture; multiple-charged particles; external mixture

APPLICATION OF A CALIBRATED AEROSOL CAVITY RING DOWN SPECTROMETER AT 355 NM FOR THE MEASUREMENT OF SCATTERING AND ABSORBING HOMOGENEOUS AEROSOLS AND AEROSOL MIXTURES

by

KIMBERLY J SCHULDT

B.S. UNIVERSITY OF PORTLAND, 2011

A Thesis Submitted to the Graduate Faculty of The University of Georgia in Partial Fulfillment of the Requirements for the Degree

MASTER OF SCIENCE

ATHENS, GEORGIA
2014

APPLICATION OF A CALIBRATED AEROSOL CAVITY RING DOWN SPECTROMETER AT 355 NM FOR THE MEASUREMENT OF SCATTERING AND ABSORBING OF HOMOGENEOUS AEROSOLS AND AEROSOL MIXTURES

by

KIMBERLY J SCHULDT

Major Professor:	GEOFFREY SMITH
Committee:	GARY DOUBERLY
	JASON LOCKLIN

Electronic Version Approved:

Maureen Grasso
Dean of the Graduate School
The University of Georgia
May 2014

DEDICATION

This work is dedicated to my wonderfully loving and supportive family: my parents, Brad and Jeanie, and my brother Christopher. They have been a source of inspiration, immeasurable patience, and support. They taught me that nothing worthwhile is easy and that nothing should be taken too seriously. These three have been such a source of strength and joy throughout my pursuit of education in ‘potions and explosions’. I would not be where I am today without these three supporting me.

ACKNOWLEDGEMENTS

The completion of this research and the compilation presented here would not have been possible without the dedication and patience of my graduate advisor Geoffrey Smith. He enthusiasm and creative knack for experiment were inspiring and motivating and taught me to be passionate about research and learning. MAJ Justin Toole provided mentorship and patience in teaching my to be an effective researcher. Additionally MAJ Toole and Lindsay Renbaum-Wolff need to be acknowledged as well for their extensive development work with the cavity ring down instrument. Lindsay Renbaum-Wolff collected some of the Snell's law data presented here. Jason Locklin and Gareth Sheppard provided the expertise and instrumentation for spectroscopic ellipsometry measurements; along with Jeremy Vanderslice from JA Woollam, who collected some of the spectroscopic ellipsometry measurements reported here.

TABLE OF CONTENTS

Page

CHAPTER

LIST OF TABLES

LIST OF FIGURES

CHAPTER ONE

CURRENT UNDERSTANDING OF THE ENVIRONMENT AND THE IMPORTANCE OF AREOSOLS IN THE GLOBAL RADIATIVE BUDGET

1.1 Atmospheric Composition

The atmosphere of the earth is as stratified as it's crust, each layer filling a unique role in the global climate system. The dynamics within each layer, and the specific role of each, are largely based on composition. For instance, 80% of the earth's ozone is found in the stratosphere; as a result, this layer prevents a majority of harmful UV radiation from reaching the surface.[1] The troposphere is the lowest layer in the atmosphere and contains most of the globe's atmospheric moisture, stored in the form of clouds, humidity, and precipitation. This is also the layer with which life on earth directly interacts; making it the first to respond to changes in composition due to activity at the surface.[1-3]

Both natural and anthropogenic sources are known to change the composition of the atmosphere through the production of greenhouse gases and aerosol particles. Their introduction into the atmosphere affects the balance of incoming and outgoing radiation. Greenhouse gases like CO_2, CH_4, and N_2O are strong absorbers of long wave radiation; these gaseous compounds were named for their ability to absorb and reemit this radiation as heat, consequently warming the planet, causing a "greenhouse effect".[4,5] Greenhouse gasses have been the topic of studies for many decades, resulting in an increased understanding of their global impact. In some cases this understanding has led to federal regulations meant to decrease their atmospheric concentrations, therefore mitigating their harmful health effects, slowing their depletion of the ozone layer, and minimizing their contribution to the greenhouse effect.[1,2,6,7] The impact of these gaseous compounds is well understood, however, the importance of aerosol particles to climate and impact on human health is still a growing area of research.

Although aerosol particles have become an important topic of study, there remains a high level of uncertainty regarding their role in the atmosphere. Some of this uncertainty can be attributed to the diversity of aerosol sources and the mixing state of the particles they generate. Volcanic activity is an example of a natural source generating a myriad of aerosol particles and gases. Within these volcanic plumes, aerosols are known to react with gaseous compounds later aggregating to form new complex particles that may then undergo photodegradation.[2,4,5] The complexity of natural sources makes it very difficult to predict the types and size of particles produced. Major anthropogenic sources of strongly absorbing aerosols are fossil fuel and biomass burning, generating aerosols that are strong absorbers of both UV and long wave radiation.[8-10] Independent of the aerosol source, their interaction with solar radiation can be described by the absorption or scattering of long and shortwave radiaiton.[11] The balance between these interactions has important impacts on the climate system.

The current scientific understanding of the atmospheric impact of greenhouse gases and ambient aerosols is presented in Figure 1.1, reprinted from the International Panel on Climate Change 2013 report. This figure presents the impact of greenhouse gases and aerosol particles as radiative forcing. Radiative forcing describes the energy difference from the top of the atmosphere to the surface based on the presence of clouds, aerosols, or gaseous compounds.[12] A positive radiative forcing represents an increase in energy due to absorption creating a warming effect; a negative radiative forcing represents energy being reflected back to space creating a cooling effect. There is a high level of certainty associated with the warming effect of CO_2, this particular compound is the single largest contributor to global warming.[7] This magnitude of this warming effect is depicted in Figure 1.1; the uncertainty associated with this forcing is a small percentage of the overall value. Similarly the uncertainty associated with CH_4 and N_2O is almost negligible when compared to the overall warming. The uncertainty associated with aerosol however is much larger. Mineral dust, for instance, is estimate to exhibit a radiative forcing of $- 0.10\ W/m^2 \pm 0.20\ W/m^2$. The uncertainty on this measurement is twice the magnitude of the forcing. Similarly, the radiative forcing of organic carbon particles is $– 0.29\ W/m^2 \pm 0.21\ W/m^2$; in this case the uncertainty is of equal magnitude to the estimated forcing. The uncertainty of these estimates reflect the need for more accurate measurements of aerosol optical properties, specifically in the UV where organic carbon exhibit is highly wavelength dependent absorption.

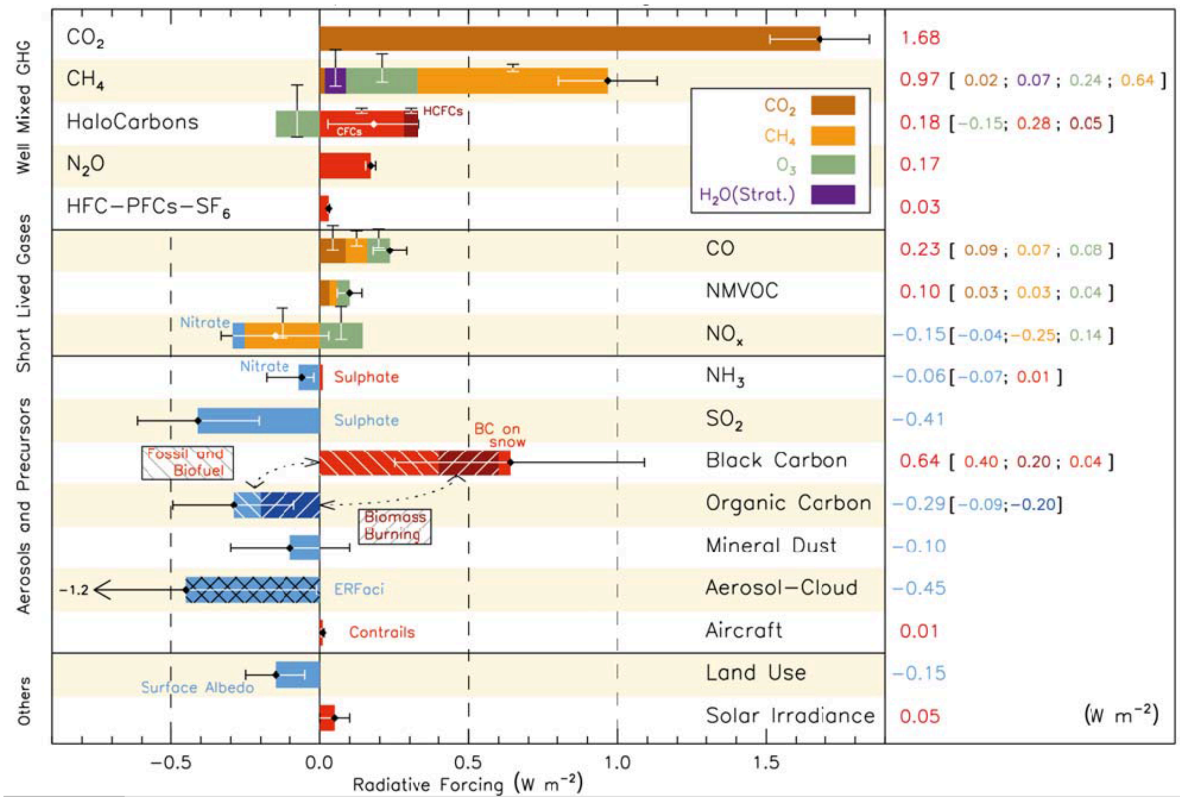

Figure 1.1 Reprinted from *Climate Change 2013: Physical Basis* associated with the by the International Panel on Climate Change.[7]

1.2 Aerosols in the Atmosphere

The role of aerosol particles in the atmosphere is described by two distinct phenomena, the indirect and direct effects. The indirect effect describes the role of aerosols as cloud condensation nuclei. Water droplets forming around an aerosol particle will reach saturation sooner than a pure water droplet leading to a higher number density of smaller cloud droplets. [13,14] The direct effect on the other hand describes the interaction of aerosol particles with incoming solar radiation.[9,15] Aerosol particles, like greenhouse gases, exhibit wavelength dependent absorption and scattering, the sum of which is called extinction. Extinction can be described by the complex refractive index, $m_\lambda = n + ik$; the real part (n) represents scattering and the imaginary part (k) represents absorption. Mie theory is a solution to the Maxwell equations that enables the prediction of the magnitude of extinction for a spherical particle of known size and index of refraction.[12] Using these wavelength specific optical properties the radiative forcing for any compound can be predicted. Much of the uncertainty associated with aerosols illustrated in Figure 1.1 comes from a lack of knowledge regarding the composition, size distribution, and mixing state of ambient aerosols.

1.3 Aerosol Measurement Techniques

Many ambient studies utilize a synergistic approach in order to a gain a more complete picture of aerosol mixing states, optical properties, and size distributions.[16,17] A study by Raut et al. presents ambient aerosol measurements collected over Paris, France using Lidar, sunphotometer, nephelometer, and aethalometer.[17] Each of these instruments has a particular niche within the study. The nephelometer, for instance, measures aerosol scattering; in combination with absorption measurements collected using the aethalometer total aerosol extinction can be estimated. Sunphotometer measurements of optical depth can be used to parameterize the analysis of Lidar data improving the accuracy of total particle concentrations. Information regarding specific aerosol composition and total concentration over Paris was retrieved based on the simultaneous measurements collected by these four techniques.[17] A study by Dinar et al. utilized filter collection in order to trap ambient particles from urban and rural locations before re-aerosolizing them and measuring the extinction cross sections (cm^2/particle) using cavity ring down spectroscopy. This procedure allowed for particle size selection enabling a complex refractive index to be fit to the extinction measurements.[18] Re-aerosolizing the trapped particles allows for size selection but sacrifices any ambient size distribution and mixing state information.

Other studies have been performed using lab-generated aerosols of select compounds of interest with the intent of improving accuracy. Many of these studies focus on the retrieval of absorption, scattering, or total extinction measurement for atmospherically relevant aerosols of a selected diameter or size distribution. A study by Lack et al. presents photoacoustic spectroscopy as a sensitive absorption technique for aerosols and gases.[19] Ma et al. reports single scattering albedo using measurements from an aerosol albedometer, an instrument measuring total extinction and scattering simultaneously.[20] Each of the studies described here present novel techniques for the measurement of specific aerosol optical properties. There are some examples of broadband cavity ring down[21] and photoacoustic[22,23] experiments reporting measurements of aerosol complex refractive indices and absorption between 350 - 440 nm. Measurements in the UV are of particular importance for organic carbon aerosols which exhibit highly wavelength dependent absorption, demonstrating its strongest absorption at wavelengths shorter than 400 nm.[10,23,24] The lack of these measurements in the literature contributes to the uncertainty in the aerosol direct effect, which propagates through to modeling studies. As a result, there remains a need for accurate measurement of aerosol optical property measurements in the UV.

From the rising temperatures observed around the globe to the increased magnitude and occurrence of severe weather, there is an apparent need for an ability to predict and forecast the state of the atmosphere.[25] Atmospheric models work to fill this need by simulating the response of the atmosphere to changes in composition. Recent modeling studies have included aerosol particles and attempted to predict their role in the changing climate.[2] A complete understanding of the aerosol direct effect is pivotal for describing the current state, and predicting the future of, the climate system.[4] However, as illustrated in Figure 1.1, there is a high level of uncertainty associated with aerosol measurements leading to a high level of uncertainty in model predictions.

1.4 Goals of This Work

Aerosol cavity ring down spectroscopy (A – CRDS) has been proven as a sensitive technique for the measurement of total aerosol extinction. [26,27] Many studies in the literature have presented measurements collected at 532 nm for compounds including ammonium sulfate and nigrosin. [28-30] Ammonium sulfate appears in Figure 1.1 as a purely scattering aerosol particle generated by both natural and anthropogenic sources. Nigrosin is a dye mixture serving as a surrogate for black carbon aerosols. Comparing the extinction cross sections measured by A – CRDS at known particle diameters to those predicted by Mie theory allows a complex refractive index to be fit. Accurate complex refractive index measurements of atmospherically-relevant particles could greatly improve the uncertainty associated with the aerosol direct effect. While literature studies at 532 nm yield valuable information in the visible there is a significantly need for accurate complex refractive index measurements in the UV. This work presents precise aerosol complex refractive indices using A-CRDS 355 nm.

The sensitivity and accuracy of the aerosol measurements presented in this work were greatly improved through the implementation of a novel calibration technique presented by Toole et al,[8] this calibration accounts for day to day systematic error the error on each extinction cross section measurement was minimized. This work will demonstrate the application of this calibration to homogeneous aerosols and aerosol mixture. In all case the percent difference between the measured complex refractive indices for pure scattering compounds compared to those predicted by Mie theory was less than 3%. The purely scattering aerosol measurements demonstrate the high level of accuracy of retrieve complex refractive indices based on the daily calibration of the CRDS instrument. Also presented here are measurements of a weakly absorbing aerosol internal mixture composed of 2-(2-benzotriazol-2-yl)-6-dodecyl-4-methylphenol (BDMP), a strong UV absorber, and squalane. The small absorption value reported for this mixture was k = 0.004 in close agreement with the absorption predicted by the volume fraction mixing rule. This mixture is a good surrogate for weakly absorbing ambient aerosols, the lower bound for these aerosols is k = 0.007 as reported by Lack et al.[23] The contribution by multiple-charged particles is also demonstrated along with the importance of mixing state through measurements of aerosol external mixtures. Finally initial result of phase dependent aerosol optical properties are described.

CHAPTER 2

CALIBRATION OF AN AEROSOL CAVITY RING DOWN INSTRUMENT

2.1 Introduction

Many techniques have been proposed for the retrieval of aerosol optical properties in the last several decades, ranging from Beer's law to more complex single particle detection techniques.[31] Few of these techniques have led to accurate measurements of refractive indices in the ultraviolet region of the spectrum. In order to build a better picture of the chemistry in the atmosphere it is important to have an accurate understanding of aerosols in the UV and visible. Among the more prominent measurement techniques are filter-based measurements and photoacoustic, nephelometry, and cavity ring down spectroscopy as *in situ* techniques.[9]

Filter-based measurements are most comparable to extended timescale Beer's law measurements where the path length is not based on the dimensions of a cuvette but instead can be thought of as the length of time air was pulled through a filter.[9] The optical properties of the collected aerosol mass are then determined through transmission spectroscopy comparing the pre-collection to the post-collection filter. Several assumptions must be made in the implementation of this type of measurement: the distribution of aerosols across the filter is uniform, particles of differing composition are randomly distributed, and observed extinction can be attributed to the aerosols not artifacts from the filter. This type of measurement is particularly susceptible to multiple scattering introduced by the filter, yielding an overestimate in the extinction caused by the collected aerosols.[9,24,32] In addition to absorption artifacts contributed by the collection filter, any morphology-specific extinction information has been lost; for example particles are often elongated and deformed when deposited onto a fibrous filter.

In contrast to filter-based measurements, *in situ* techniques measure aerosols suspended in air, eliminating filter artifacts allowing the impact of particle morphology and composition to be observed. Examples of *in situ* measurement techniques are nephelometry and photoacoustic spectroscopy; these techniques isolate either scattering or absorption. Photoacoustic spectroscopy measures absorption by detecting the intensity of thermal expansion and relaxation; measured as a thermal acoustic wave; when light of a chosen wavelength vibrationally excites molecules; if the concentration is known an absorption coefficient is reported. [19,24] Nephelometry measures the scattering of light at the chosen wavelength and when coupled with a concentration measurement, like particle number density, a scattering coefficient is reported. Each of these measurements is valuable but neither yields a complete picture.

This work has enlisted pulsed cavity ring down spectroscopy, CRDS, as an *in situ* measurement technique that directly measures total particle extinction, the sum of both absorption and scattering. Utilizing CRDS and Mie theory allows for the retrieval of aerosol complex refractive indices. Mie theory describes how a spherical particle of a known refractive index will interact with a specified wavelength of light.[33] Utilizing the particle diameter and refractive index Mie theory predicts the observable extinction. By comparing the measured extinction cross sections to Mie theory predictions at a known wavelength and diameters a complex refractive index can be retrieved.[28,34,35] This technique, "reverse" Mie theory, is typically used in aerosol cavity ring down experiments.[36-38]

In recent years CRDS has greatly increased in popularity both for the simplicity of design as well as the versatility of application. CRDS has been used to study the optical properties of coated aerosols,[39] the change in deliquescence point based on relative humidity,[40] and in conjunction with other detection techniques to deliver accurate measurements of single scattering albedo.[41] While the breadth of this application is impressive, few studies have led to precise measurement of aerosol complex refractive indices in the ultraviolet. There are several studies at 532 nm[36-38] but very few at 355nm; this shortage is not limited to CRDS.[8,20,42] As discussed in the previous chapter, there is a high degree of uncertainty regarding aerosol optical properties. Unfortunately, current literature regarding the improvement of CRDS measurements is limited, and to date there have been two publications pertaining to calibration in CRDS instruments Miles et al and Toole et al. [8,43] By accounting for systematic error as described by Toole et al the accuracy of aerosol refractive indices retrieved by cavity ring down at 355nm has greatly improved.[8]

2.2 CRDS as an *in situ* Technique

Pulsed cavity ring down requires only a radiation source, an optical resonator or ring down cavity, a photodetector, and an oscilloscope or personal computer to process the signal. The optical resonator is made up of two dielectric coated highly reflective mirrors, between which radiation will resonate, i.e. ring down. A pulsed laser sends radiation into the front mirror; for each laser pulse a small percentage of light leaks into the ring down cavity. The light then bounces back and forth between the mirrors leaking a small percentage out the back mirror to be detected by a photomultiplier tube, PMT, at each pass.[26,27,44,45] The PMT signal is displayed on an oscilloscope and an exponential decay function is fit. The decay rate, τ, is referred to as the ring down time; i.e. the length of time, typically in ns, required for the signal to decay to zero.

$$I = I_o e^{-\alpha_{ext} L} = I_0 e^{-\frac{\tau}{\tau_0}} \tag{1}$$

Here α is the total extinction; L is the length of the cavity; τ and τ_0 are the ring down times with and without aerosols. The ring down time will be longest when the cavity is empty, referred to as τ_0. When a gas or aerosol particles are flowed into the cavity the ring down time will decrease due to light scattering and absorption. In the case of gases, absorption is the only observable form of extinction; for aerosol particles however, both absorption and scattering are observed. Similar to Beer's law, cavity ring down spectroscopy utilizes the difference in empty versus occupied ring down times to determine the total extinction, α_{ext}.

$$\alpha_{ext} = \frac{R_L}{c}\left(\frac{1}{\tau} - \frac{1}{\tau_0}\right) \tag{2}$$

The equation above demonstrates the relationship between empty and occupied ring down times, τ and τ_0 respectively, and the ratio between the total cavity length and the length over which particles interact with light, R_L. As seen in Figure 2.1 the particle inlets to the cavity are set at a 45° angle and are offset from the ends: in addition, a purge flow over the mirrors prevents any backflow of particles toward them limiting the length of particle light interaction. Normalizing the total extinction by the particle number density, N, the extinction cross section, σ_{ext}, can be calculated.

$$\sigma_{ext} = \frac{\alpha_{ext}}{N} \tag{3}$$

The extinction cross section can also be calculated for any refractive index and particle diameter using Mie theory. Mie theory describes how effectively a particle of known diameter and refractive index can absorb or scatter light of a particular wavelength.[33,46] This study minimizes the number of assumptions required to employ Mie theory, specifically that particles are spherical, homogeneous, and monodisperse. Choosing compounds with low vapor pressures and melting points it is safe to assume the particles generated are spherical and do not evaporate over the length of the measurement region.

2.3 Aerosol Cavity Ring Down Instrument Description

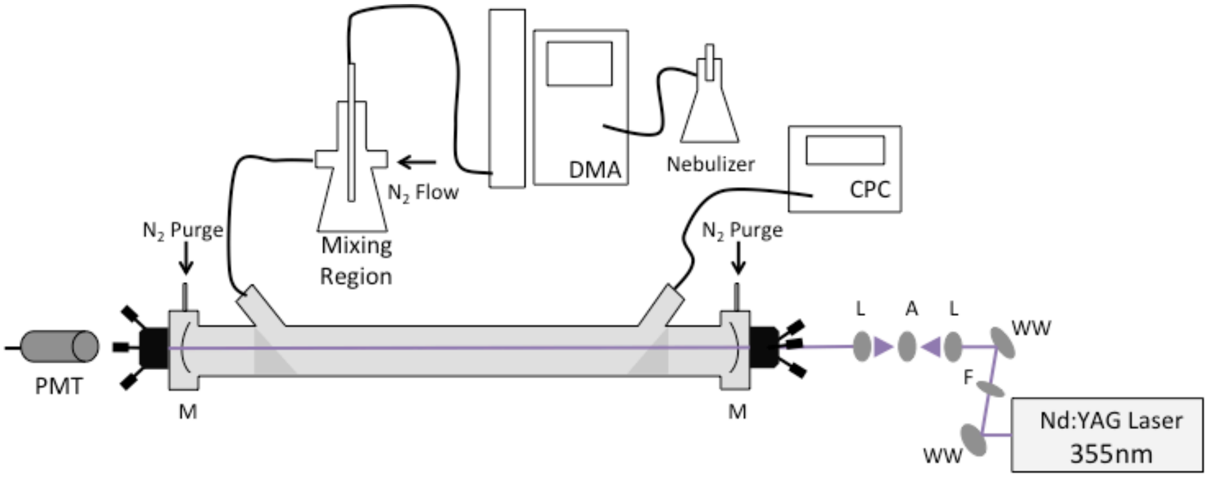

Figure 2.1 Aerosol cavity ring down instrument diagram. L are lenses, WW are wedge windows, A is a pinhole aperture, F is a UV filter, M are 99.99% reflective concave mirrors coated for modal reflectivity at 365nm, DMA is the differential mobility analyzer, CPC is the condensation particle counter.

Cavity Ring Down Cell and Radiation Source

The cavity ring down cell is made up of a 103.1 cm aluminum tube with dielectric concave mirrors coated for 99.99% reflectivity centered at 365 nm. The third harmonic of the Nd:YAG laser pulses 355 nm radiation into the cavity at 10 Hz. Radiation leaving the laser first passes through a UV filter, isolating the 355 nm radiation, before entering the spatial filter. The spatial filter is a telescoping setup that selects for the TEM_{00} transverse mode before the light enters the cavity, in turn improving the stability of the signal.[26] Both the spatial filter and curvature of the mirrors ensure a monoexponential decay. The exponential character of the decay is important for accurately fitting the ring down time in the presence of particles.

Particle Generation

Particles are generated using a concentric nebulizer. A 0.030- 0.040 lpm flow of dry nitrogen is passed through the nebulizer pulling liquid from a reservoir generating a polydisperse, log normal, particle distribution centered around 400 nm.

Size Selection

Aerosol particles flow into a TSI differential mobility analyzer, DMA (TSI 3080), at a flow rate of 0.27 lpm. Particles enter the DMA through a 0.508 cm inertial impactor, which has a D_{50} of 915 nm. Based on the momentum of incoming particles the 50% cut-point diameter, D_{50} of 950nm, is the diameter at which 50% of incoming particles are lost. Within the DMA particles of the desired diameter are selected based on their electrical mobility. A charge is first imparted to the particles when the aerosol passes through a radioactive Krypton source and into the selection region. The selection region is made up of a central electrified rod and grounded outer wall: a voltage is applied to the central rod according to the diameter of interest. The resulting voltage gradient allows the desire particles to pass while all others will collide with the central rod or be lost to the outer wall.[47] Exiting the selection region is a monodisperse particle distribution centered on the selected diameter, with a geometric standard deviation of 1.050 as specified by the manufacturer. This monodisperse distribution then flows into the mixing flask where flow balancing dry nitrogen is introduced before particles are introduced into the measurement region. All experiments in this work are conducted with particle diameters between 600 and 900 nm. Based on the impactor cut point, $D_{50} = 915$ nm, it is safe to assume the no multiply-charged particle will be observed in the measurement region.

Particle Concentration

Upon exiting the CRD cell the particle number density is measured utilizing a butanol-based TSI condensation particle counter, CPC (TSI 3775). After entering the CPC particles flow through a heated growth region where they are grown based on condensation of supersaturated butanol vapor. The larger, grown particles are then counted as they flow past an optical counter and a number density is reported.

Signal Acquisition

The ring down signal is detected by a PMT (Hamamatsu 63500) and sampled using an oscilloscope (HP 5483). The decay function is fit by a custom LabVIEW program and the ring down time reported. The same program calculates the total extinction, reports the particle number density, and calculates the extinction cross section. The decays are collected at one second averages in the LabVIEW program, the extinction cross section is calculated in real time and a rolling average is recorded every two minutes, 200 laser shots, for a minimum 8 minutes per diameter, or 4 data points. At each

2 minute mark the extinction cross section, particle number density, and cross section standard deviation are recorded. The cross section and standard deviation will be used later in a Mathematica reverse Mie fitting routine.

2.4 CRDS Calibration with Squalane

The CRDS is calibrated with squalane daily in order to account for systematic errors. Squalane has a well-characterized refractive index of 1.472+0.00i. In this calibration step, extinction cross sections are collected for 5-7 selected diameters and compared the values predicted by Mie theory. Through an iterative process, a scaling factor, Cf, and diameter shift, Δd, are imposed on the collected data points shifting them to achieve the best fit with the known extinction cross sections predicted by Mie theory.[8] Each iteration imposes a combination of Cf and Δd on the data; these new effective cross sections, σ_{ext},[8] are then compared to the extinction cross sections predicted by Mie theory, σ_{Mie}, at the original diameters. The fitness of each combination is assessed by chi-squared, where ε_{ext} represents the variance,

$$\chi^2 = \sum_{i=1}^{N} \frac{(\sigma_{ext} - \sigma_{Mie})_i^2}{\varepsilon_i^2} \tag{4}$$

The values of Cf and Δd are varied over a range of 0.75 - 1.25 and -40 - 40 nm, respectively, the combination returning the minimum chi-square best fits the data the predicted σ_{Mie} values. Values for Cf and Δd typically lie in the range of $0.95 < Cf < 1.15$ and $14\text{ nm} < \Delta d < 28\text{ nm}$. Careful selection of the measurement diameters ensures those chosen are at points in the refractive index curve where the size distribution information can be obtained. The sizes selected are specific to squalane and new sizes, within the 600 to 900 nm range; alternative sizes may be better suited for other calibrants. An example of the applications of Cf and Δd to a set squalane data is shown in Figure 2.2. Here Cf and Δd are 0.988 and + 20nm, respectively, and improve the average σ_{ext} error from 2.14% to 0.91%.

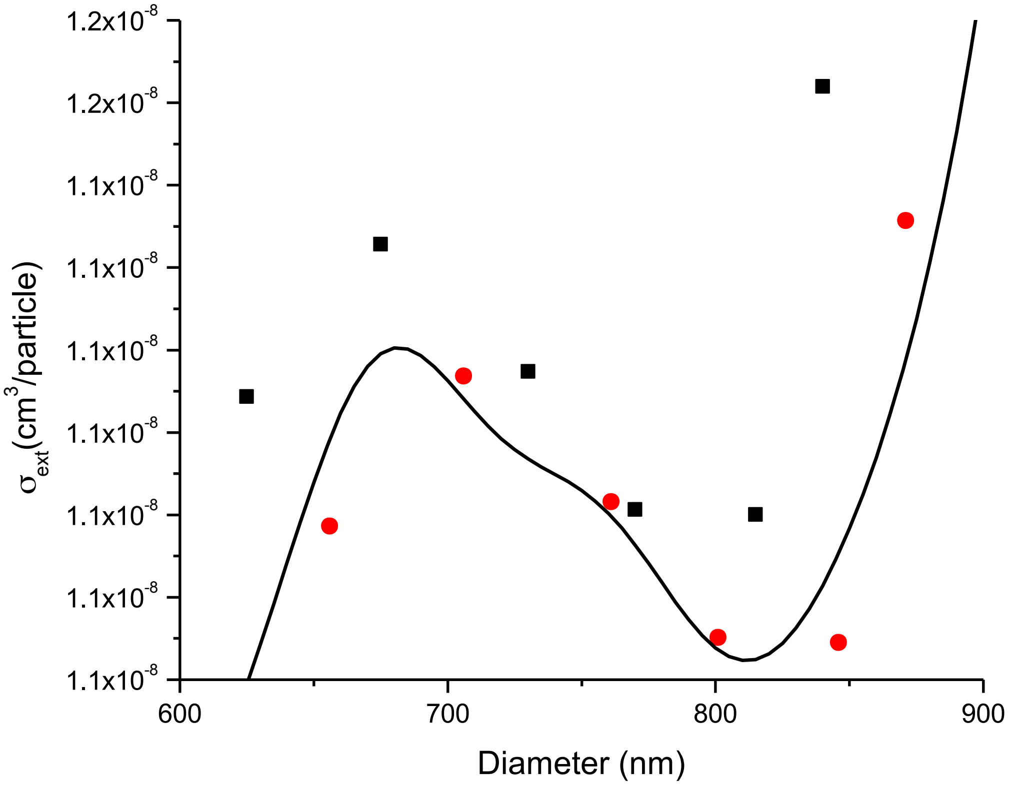

Figure 2.2 Application of calibration factors, Cf and Δd, to squalene σ_{ext} data. Square black markers represent raw σ_{ext} data, red circular markers represent σ_{ext} shifted by Cf= 0.988 and Δd= +20 nm, solid line represents m_{λ}=1.472+0.00i. σ_{ext} error improved from an average 2.14% to 0.91% with calibration.

Application of Calibration to Measurements with Other Aerosols

Calibration factors remain consistent throughout enabling their application to measurements of other aerosol species. Similar to the procedure for squalane, a different aerosol species is nebulized, 5-7 diameters are selected, and the extinction cross sections retrieved. The calibration factors from the squalane calibration are then imposed on the measured cross section values and new effective cross sections are returned. These values are then fed into a reverse Mie calculator, a Mathematica fitting algorithm, where a refractive index is determined. This fitting routine is an iterative process comparing the new effective cross section values to cross sections predicted by Mie theory, in this case each iteration predicts cross section values for variable of n and k values within the defined range. Chi-squared values are reported for each comparison as an assessment of the fitness. The best 'fit' refractive index returns the lowest chi-squared value. Figure 2.3 shows the application of calibration factors to a set of squalene data. The calibration factors applied are the same as those derived from the squalane calibration in Figure 2.2, Cf = 0.988 and Δd = +20 nm.

Importance of Calibration

The scaling term, Cf, accounts for under or over counting by the CPC, anomalies in particle mixing and flow, as well as uncertainties in R_l. Toole et al. showed that variations in the mixing region can affect the reported Cf, supporting the claim that turbulent flows may impact the reported σ_{ext} values[8]. A recent study conducted by Collins et al. indicated that CPC undercounting, due to coincidence, may be observed in experimental conditions of high particle concentrations, 20,000-40,000 particles/cm^3.[48] The majority of CRDS experiments are performed using concentration below 1000 particles/cm^3 but concentration in the 20,000 particles/cm^3 range may be observable during extreme pollution events. Similarly, Miles et al. recently reported that error in R_L

could lead to an uncertainty of as much as 2.5% in retrieved refractive indices.[43] Both of these studies, along with Toole et al., support the need for calibration.

The diameter shift, Δd, accounts for selection error imposed by the DMA.[8] Toole et al. showed that this error is specific to each DMA and relatively consistent from day to day implying manufacturer error[8]. This cannot be attributed to an internal error in the DMA as the flows through the system, and in the DMA particularly, are carefully regulated. Miles et al reported that calibration with polystyrene latex spheres can contribute as much as 2.9% error in the retrieved refractive index of aerosols due to the manufacturer's ±6 nm tolerance on the quoted diameter.[43] Calibrating with squalane is advantageous in that particles selected will behave in the DMA similarly to the aerosols the calibration is applied to. Calibrating in the manner above improved the average percent error on the cross section measurements of squalene shown in Figure 2.3 from 1.82% to 0.59%. The refractive index fit to collected data before Cf, 0.988, and Δd, +20 nm, were applied to the squalene data was 1.529 + 0.010i. This fit is particularly troubling because squalene does not absorb in the UV. After the calibration factors were applied, the best-fit refractive index was 1.533+0.00i. This is in close agreement with literature refractive index values for squalene[49] (m = 1.529+0.00i)xs. Further evidence of improvement in retrieved refractive indices due to calibration is discussed in Chapter Three.

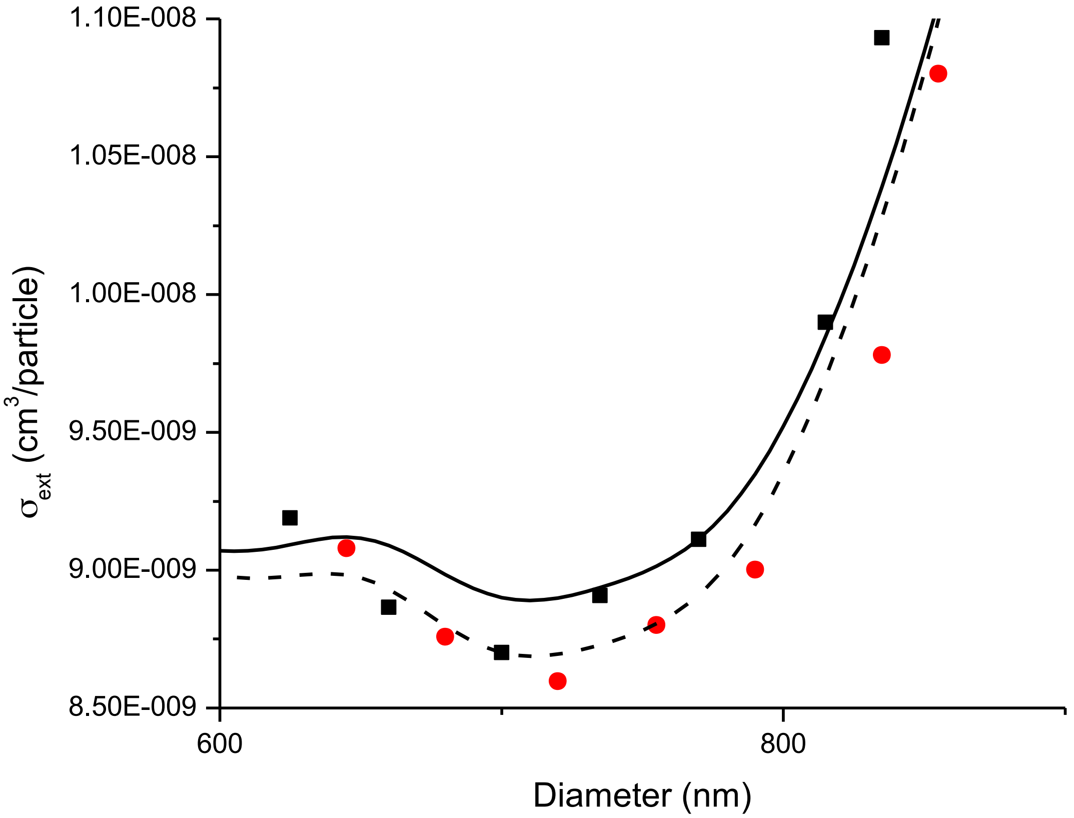

Figure 2.3 Squalene σ_{ext} data adjusted to Δd and C_f calibration factors. Refractive index error improved from 1.82% to 0.59% after application of calibration factors. The solid line represents m_λ=1.529+0.003i fit without calibration; corresponding to the square black markers representing raw σ_{ext} data. The dashed line represents m_λ=1.533+0.00i, the red circular markers representing the shifted σ_{ext} using Cf= 0.988 and Δd= +20 nm. The reported refractive index for squalene at 355 nm is 1.529+0.00i.[50]

2.5 Comparison to Bulk Measurements

The refractive index of squalane is verified using several bulk techniques discussed below, each measures squalane in the absence of the DMA and CPC eliminating any systematic error imposed by the size selection and particle counting instruments. Other CRDS studies do not calibrate the CRDS instrument, but instead use polystyrene latex spheres, PSLs, to validate the instrument, quoted refractive indices range by 2.7%.[43] Miles et al. discusses the danger of using PSLs as a calibrant[43]. The refractive index of PSLs is not measurable in the bulk state, limiting the possibilities of verification of manufacturer refractive index, an uncertainty on this measurement could result in as much as 0.3%- 0.5% uncertainty on retrieved refractive indices[43].

The refractive index of squalane was measured by each of the measurement techniques described below. This is possible because squalane is a homogeneous liquid, unlike PSLs that are particles suspended in solvent. Each of these techniques was validated using common solvents and subsequently used in the retrieval of refractive indices for squalane, squalene, dicotyl sebacate (DOS), and oleic acid. Like squalane, the latter three compounds do not absorb UV light, they have low vapor pressures and melting points, and they form spherical particles when aerosolized. All three of these compounds have appeared in aerosol CRDS studies at 532 nm,[37,39,51] both as homogeneous particles and as aerosol coatings, where an accurate refractive index is especially important.

Snell’s Law

A custom fabricated Snell’s law cell was enlisted as an alternative method for the measurement of bulk refractive indices. The cell was a custom fabricated aluminum box with a single window in the back and two windows offset at a fixed 14.84° angle in the front. A diode laser centered at 532 nm and a HeNe at 633 nm were used as the light sources, Figure 2.4. Measurements at 355nm were collected using the third harmonic of an Nd:YAG laser[*]. The incident beam was split by a dichroic, DC, the unchanged portion traveling straight through the cell while the reflected portion was aligned perpendicular to the angled window using an aluminum mirror.

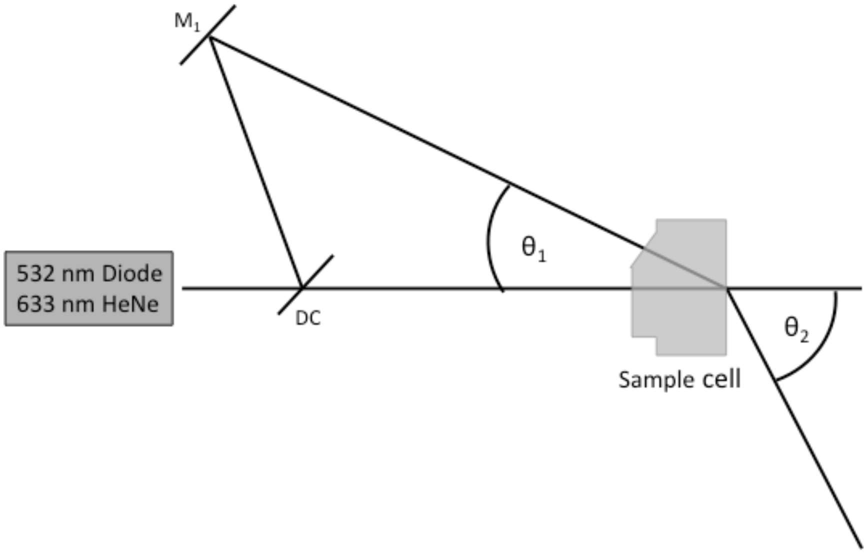

Figure 2.4 Snell's law cell diagram. θ_1 fixed 14.84° angle between incident beams, θ_2 angle dependent on presence of analyte. M_1 is the aluminum mirror used to reflect light from the dichroic into the angled window at the front of the sample cell.

In the absence of any analyte, the incident beam angle, θ_1, and exiting beam angle, θ_2, are equivalent (see Figure 2.4). When an analyte is introduced into the cell, the angle of the beam exiting the cell, θ_2, will increase. Assuming the refractive index of air, m_1 = 1.00, the retrieval of a refractive index for the analyte, m_2, becomes a simple trigonometric expression (Snell's Law):

$$m_1 \sin\theta_1 = m_2 \sin\theta_2 \tag{5}$$

Solvents with well-known refractive indices, like methanol, ethanol, and acetonitrile were used to validate the technique before measurement of CRDS. Validation compounds

---

[*] Measurements at 355nm were collected by Lindsay Renbaum-Wolff

include squalane, oleic acid, and dioctyl sebacate (DOS). The results of these measurements are presented in Table 2.1.

Abbè Refractometry

Abbè refractometry is a refractive index technique dating back to 1874. In this particular technique a liquid sample is pressed between a refracting prism of high refractive index and a ground glass slide in the sample region. The bottom slide ensures a light and dark region upon illumination of the sample. An external light source shines through the lower ground glass slide illuminating the sample. Adjusting the boundary of total reflection, the light and dark region, to the indicated position in the eyepiece allowing a refractive index to be read from graduations on fine and course adjustment dials.[52]

Spectroscopic Ellipsometry

The spectroscopic ellipsometer is a commercial instrument produced by JA Woollam. This instrument directly measures changes in the amplitude, ψ, and phase, Δ, of incident radiation leaving the sample cell both with and without analyte present. In this case analyte was pushed through a flow cell atop a silicon wafer. The relationship between ψ and Δ measurements at many wavelengths correspond to the ratio of reflectance for p and s polarized light, r_p and r_s respectively,

$$\rho = \frac{r_p}{r_s} = \tan\psi \bullet e^{\Delta i} \tag{6}$$

CompleteEASE software from JA Woolam utilizes the Fresnel approximations in order to translate the reflectance of p and s polarized light from the surface of the silicon wafer through the analyte into refractive index values. [53,54] The Fresnel approximations are shown here,

$$R_p = \frac{r_{1,2}^p + r_{2,3}^p e^{-j2\beta}}{1 + r_{1,2}^p r_{2,3}^p e^{-j2\beta}} \tag{7}$$

$$R_s = \frac{r_{1,2}^s + r_{2,3}^s e^{-j2\beta}}{1 + r_{1,2}^s r_{2,3}^s e^{-j2\beta}} \tag{8}$$

$$\beta = 2\pi\left(\frac{t}{\lambda}\right) N_2 \cos(\phi_2) \tag{9}$$

$$r_{1,2}^{p,s} = \frac{N_2 \cos(\phi_1) - N_1 \cos(\phi_2)}{N_2 \cos(\phi_1) + N_1 \cos(\phi_2)} \tag{10}$$

N represents the complex refractive index of the silicon wafer and analyte, $r_{1,2}^p$ or $r_{1,2}^s$ indicate the reflection of p or s polarized light at the interface between the analyte and the wafer, and λ represents wavelength. A Cauchy dispersion model is then fit to the real part (n) of the refractive index, while an Ubrbach equation is used to model the imaginary part (k)

$$m_\lambda = a + \frac{b}{\lambda^2} + \frac{c}{\lambda^4} \tag{11}$$

$$k = k_0 e^{D(E-B')} \tag{12}$$

where a, b and c in the Cauchy dispersion and k_0 and D in the Urbach equation are experimentally determine coefficients. Spectroscopic ellipsometer experiments were conducted with the assistance of Gareth Sheppard and Jason Locklin. A second set of ellipsometer measurements were collected by the instrument manufacturer, J.A. Woollam. These two sets of values are reported in Table 2.1. As with previously discussed bulk refractive index techniques, the accuracy of this method was first validated with well-known solvents before performing measurements with compounds relevant to CRDS

Table 2.1 Bulk refractive index measurements collected with a Snell's refractio law, Abbè refractometery and spectroscopic ellipsometry at 355, 405, 532, and 633 nm. Reported values are in close agreement with literature values, also displayed for each compound. Dashes indicate the absence of measurements in these experiments or in the literature.

Compound	355 nm[†]	405 nm	532 nm	633 nm	Source
Methanol	1.343	1.337	1.330	1.327	Kozma et al.[‡][50]
	1.342	—	1.332	1.334	Snell's Law
	—	1.329	1.329	1.328	Abbè
	1.343	1.335	1.365	1.362	Ellipsometer
	1.346	1.339	1.331	1.327	Woollam
Ethanol	—	—	1.364	1.360	Rheims at al.[52]
	1.36	—	1.362	1.360	Snell's Law
	—	1.363	1.366	1.363	Abbè
	1.379	1.373	1.365	1.362	Ellipsometer
Acetonitrile	1.359	1.353	1.344	1.341	Kozma et al.[50]
	1.356	—	1.346	—	Snell's Law
	—	1.344	1.346	1.343	Abbè
Squalane	1.471	1.465	1.454	1.450	Painter[§][49]
	1.472	—	1.452	1.449	Snell's Law
	—	1.450	1.455	1.450	Abbè
	1.469	1.462	1.453	1.450	Ellipsometer
	1.471	1.462	1.451	1.447	Woollam
Squalene	1.521	1.509	1.495	1.487	Painter[49]
	—	—	1.492	—	Snell's Law
	—	1.494	1.497	1.492	Abbè
	1.465	1.491	1.501	1.497	Ellipsometer
	1.528	1.514	1.498	1.4467	Woollam
DOS	—	—	1.455[37]	—	Reference
	1.469	—	1.449	1.447	Snell's Law
	1.470	1.461	1.451	1.446	Woollam
Oleic Acid	—	—	—	—	Reference
	1.483	—	—	—	Snell's Law
	—	1.457	1.460	1.458	Abbè

[†] All Snell's law measurements at 355 nm were collected by Lindsay Renbaum-Wolff

[‡] Kozma (2005) refractive indices were collected via GVM, Cauchy and Sellmeier dispersions.

[§] Painter(1984) refractive indices were measured via electron scattering measurements

2.6 Conclusions

Previous studies demonstrating the use of cavity ring down spectroscopy for the retrieval of aerosol complex refractive indices use PSLs to validate the accuracy of the instrument.[28,37,38] Several assumptions must be made in this validation: that the manufacturer quoted diameter and distribution are accurate, that the quoted refractive index is accurate, and that the instrument performance does not change after validation. There are several issues with this type of validation namely there is a 2.7% variance on reported refractive indices for polystyrene latex spheres in the literature, manufacturer quoted diameters can vary up to ±6nm,[43] and this validation does not account for day to day changes in experimental conditions.

Toole et al. demonstrated the importance of daily calibration in order to account for systematic error associated with flow conditions, size selection, CPC counting efficiency, and uncertainties in R_L. Frequent calibration led to an improvement in the average error on retrieved extinction cross section values from 10.6% to 1.6%.[8] In contrast to PSLs the refractive index of the chosen calibrant, squalane, can be validated by measurements in the absence of size selection processes and without the CRDS eliminating any systematic error imposed by these processes. The bulk measurements discussed in this chapter validate the reported 1.472+0.00i refractive index for squalane.

Much of the problem with PSLs is the inability to validate the refractive index without aerosolizing, size selecting and employing CRDS. If PSLs were to be used as a calibrant any systematic error would be compounded in retrieved refractive indices for other aerosols. The 2.7% variance in reported PSL refractive indices alone would lead to an uncertainty of 0.3—0.5% on refractive indices retrieved for other compounds.[43]

Additionally the manufacturer's quoted size distribution can range by ±6 nm, leading to an uncertainty in retrieved refractive indices of 2.9%.[43] By calibrating with a compound whose refractive index can be validated through alternative methods any systematic error imposed by the cavity ring down system can be accounted for.

The calibration minimizes the error between collected extinction cross sections of selected particles to those predicted by Mie theory. In order to minimize this difference a scaling term, Cf, and diameter shift, Δd, are applied to the collected extinction cross section measurements. The scaling term, Cf, accounts for uncertainties R_L, CPC counting efficiency, and turbulent flow conditions. The diameter shift, Δd, accounts for size selection error.[8] The best combination of these two parameters will shift the data closest to the extinction cross sections predicted by Mie theory. Squalane is the calibrant presented in this work. Extinction cross section measurements for particles selected are therefore compared to Mie theory predictions for complex refractive index 1.472 + 0.000i.

The complex refractive index of squalane, 1.472 + 0.000i, has been validated by several bulk methods including Snell's law, Abbè refractometry, and spectroscopic ellipsometry. Snell's law compares the angle of refraction as light travels through the compound of interest. Abbè refractometry measures angle of total reflection as diffuse light passes through the sample and the refracting prism. Finally, spectroscopic ellipsometry compares the magnitude and polarization of light after interaction with the compound of interest. Each of these measurement techniques collects measurements without aerosolizing the compound of interest and in the absence of size selection, particle counting, and CRDS. This type of measurement serves as a validation for the complex refractive indices measured with CRDS. The complex refractive index for squalene is presented in Table 2.1 along with several other compounds, in addition to squalane. Extinction cross section measurements of squalene presented in Figure 2.3 indicate that the application of the vertical and horizontal shifts, determined using squalane improved the accuracy of the retrieved complex refractive index from 1.529 + 0.003i to 1.533 + 0.000i. The importance of the erroneous absorption will be discussed further in Chapter Three.

Toole et al. has shown these calibration factors may vary by as much as 4% over the course of a day[8] but may show higher variability day to day. In order to retrieve refractive indices with a low level of uncertainty, the cavity ring down instrument should be calibrated daily rather than irregularly validated. Additionally, the importance of validation by alternate methods was presented. Validation without the need to aerosolize the compound of interest and in the absence size selection, particle counting, and CRDS minimizes systematic error associated with these measurements. The application of this calibration technique to single and multicomponent aerosols will be discussed in more detail in Chapter Three.

CHAPTER 3

ABSORBING AND SCATTERING AEROSOL COMPLEX REFRACTIVE INDICES MEASURED USING CALIBRATED CAVITY RING DOWN SPECTROMETER AT 355 NM

3.1 Introduction

Here calibrated cavity ring down spectroscopy (CRDS) is utilized for the measurement of complex refractive indices for scattering and absorbing aerosols. Careful calibration greatly improves the sensitivity and accuracy of CRDS extinction cross section measurements minimizing the occurrence of absorption values (k) fit to otherwise purely scattering compounds. Many studies using CRDS at 532 nm have reported false absorption values ranging from k = 0.0[28] - 0.01[55] for ammonium sulfate and 0.005[28] - 0.01[18] for polystyrene latex spheres (PSL). These erroneous absorption values are particularly troubling due to the relative importance of the compounds they're associated with. PSLs are a common aerosol used for validation of CRDS accuracy and are discussed in detail in Chapter Two. Ammonium sulfate is an important natural and anthropogenic aerosol that appears in a majority of atmospheric modeling studies; a small absorption value associated with the complex refractive index would incorrect skew any prediction made using these models.

Erlick et al. describes the meaningful impact a small k value has on the radiative forcing efficiency (RFE) of aerosol particles.[56] The RFE describes how well a particle will reflect incoming radiation out of the atmosphere, therefore preventing radiation from entering the climate system and in turn contributing a cooling effect. For instance, a purely scattering ammonium sulfate aerosol, with k = 0.00, will exhibit a -26.33 W/m^2 RFE; an aerosol with an absorption of k = 0.014, under the same conditions, will exhibit a -19.20 W/m^2 RFE.[56] That equates to a 25% difference in the aerosols radiative forcing efficiency, indicating that even a small false k can dramatically change the expected contribution of a particle to the Earth's radiative balance. Erlick et al. does not discuss however, the impact of overestimating k for absorbing particles.

The most dramatic example of CRDS reporting overestimated k values comes from a study by Riziq et al. measuring a 1:500 rhodamine 590:ammonium sulfate (Rh-590:AS) absorbing mixture. In this study the reported absorption was k = 0.103, 13x larger than the predicted k = 0.008.[28] This overestimate could be attributed to systematic error in the instrument or may indicate a breakdown in the mixing rules used for prediction. Other mixtures measured in this experiment reported were also fit to absorption values larger than the predicted, however the magnitude of this overestimate was not correlated with concentration. Had the measured absorption agreed with the predicted the Rh-590:AS mixtures presented by Riziq et al. would have been a good model for ambient absorbing aerosols.

According to Lack et al. the typical range for k values observed in ambient aerosols is 0.01 – 0.71.[23] While compounds like nigrosin, k = 0.26,[57] and Suwannee River fulvic acid (SRFA), k = 0.02, are good models for strongly absorbing ambient aerosols, few studies report absorption smaller than k = 0.02. A study by Dinar et al. reported the complex refractive index for absorbing ambient particles as 1.561 + 0.004i at 532 nm.[18]

That same study, however, reported the complex refractive index of PSLs as 1.597 + 0.005i.[18] The false absorption fit to PSLs, a pure scatterer at 532 nm, was almost equivalent to the absorption value reported for ambient aerosols. This suggests the ambient measurement may be at or below the instrument detection limit, limiting the reliability of the reported absorption values.

All of the literature values referenced so far in this chapter were measured at 532 nm. These studies report complex refractive indices for purely scattering particles, many of which include small erroneous absorption values, these particles serve as a model for scattering aerosols in the atmosphere. Other common compounds in CRDS studies are nigrosin, a highly absorbent dye, and Suwanee River fulvic acid (SRFA) each function as models for black and organic carbon aerosols, respectively. Black carbon particles are soot-like aerosols generated in high temperature combustion, exhibiting strong absorption at all wavelengths. Organic carbon aerosols, on the other hand, are produced by low temperature combustion and are strong absorbers in the UV, exhibiting a sharp drop off in the visible.[58] Studies conducted at 532 nm cannot accurately measure the contribution of these aerosols to overall extinction. Kirchstetter et al. reports the imaginary part of the complex refractive for organic carbon at 350 nm is k = 0.168 swiftly decreasing to k = 0.030 at 550 nm. Black carbon on the other hand has a more stable absorption of k = 0.77 at 350 nm and k = 0.72 at 550 nm.[58] This demonstrates the need for more precise measurements in the UV as well as the need for more precise measurements of weakly absorbing aerosols in all regions of the spectrum.

This work presents a complex refractive index measurement for purely scattering homogeneous aerosols with refractive indices ranging from 1.471 + 0.0i to 1.529 + 0.0i.

The complex refractive indices measured were in close agreement with the bulk measurements present in Table 2.1. The uncertainty on extinction cross section measurements for these scatterers represents less than 2% of the overall measurement demonstrating the fine precision necessary to accurately fit a complex refractive index. The CRDS was then utilized for the measurement of internally mixed aerosols testing the accuracy of the volume fraction mixing rule for the prediction of scattering and absorbing aerosol mixtures. Finally complex refractive indices are measured for a model absorbing aerosol mixture reporting k values ranging from 0.004 to 0.028. The mixtures presented here demonstrate the sensitivity of this technique to weakly absorbing aerosols.

3.2 Measurement of Complex Refractive Indices

As described in Chapter 2, aerosol particles are generated from a reservoir of compound using a concentric nebulizer. Particles are then size selected using a differential mobility analyzer before flowing into the CRD cell where they interact with 355 nm light. Finally, they flow into a condensation particle counter where particles are counted and a number density is reported. A custom LabVIEW program then calculates the extinction cross sections in real time using the total observed extinction and the reported number density. Lastly, the extinction cross sections along with the scaling factor, C_f, and diameter shift, Δd, determined in the squalane calibration, are input into a custom Mathematica reverse Mie fit program. This program scales the collected cross sections according to the calibration factor and determines the best-fit combination of n and k for the effective extinction cross sections.

3.3 Scattering Aerosols

Scattering compounds presented include squalene, oleic acid, dioctyl sebacate, and a Cargille immersion liquid. Excluding the Cargille immersion liquid, the refractive index for each of these compounds was validated using the bulk methods described in Chapter 2, including Abbè refractometry, Snell's law, and spectroscopic ellipsometry. These compounds were selected for their low vapor pressures, viscosities, and melting points. These physical properties ensured that the compounds could be nebulized and would form spherical particles that would not evaporate over the length of the CRD cell.

Squalene has a known complex refractive index of 1.528 + 0.000i at 355 nm.[49] Dioctyl sebacate (DOS) and oleic acid have appeared in aerosol mass spectrometry[59] as well as CRD studies serving as models for organic carbon coatings found on ambient particles.[39] The refractive indices of DOS and oleic acid are 1.470 + 0.000i and 1.483 + 0.000i (see Table 2.1). The Cargille immersion liquid is a mixture of compounds manufactured for a refractive index of 1.550 + 0.000i at 355 nm, calculated using manufacturer provided Cauchy equation.

Measured Scattering Aerosol Complex Refractive Indices

The refractive indices measured using cavity ring down spectroscopy at 355 nm are presented as the circular blue markers in Figure 3.1, where the reported refractive indices are compared to literature. In the absence of literature values the CRD refractive index is compared to a bulk method, like spectroscopic ellipsometry or Snell's law, with the exception of the Cargille immersion liquid which is compared to the manufacturer's specifications. All points measured here lie on the 1:1 diagonal demonstrating a close agreement between the measured and reference refractive indices. Presented error bars indicate n and k values within the 68 percent confidence interval, specified as all complex refractive index values returning $\chi^2 < \chi_0^2 + 1$ where χ_0^2 indicates the values of the chi-squared merit function for the best fit n and k values.[8] The error bars shown in Figure 3.1 are artificially small because they neglect uncertainty on the calibration factors applied to the extinction cross sections prior to fitting. The lack of empty blue markers in Figure 3.1 indicates all best fit complex refractive indices included absorption of k = 0.000, all error on these measurements was less than 0.001. This result is expected because all compounds listed above are pure scatterers at 355 nm. Unlike measurements reported in the literature, none were fit to false absorption values due to the precision of the measured extinction cross sections.

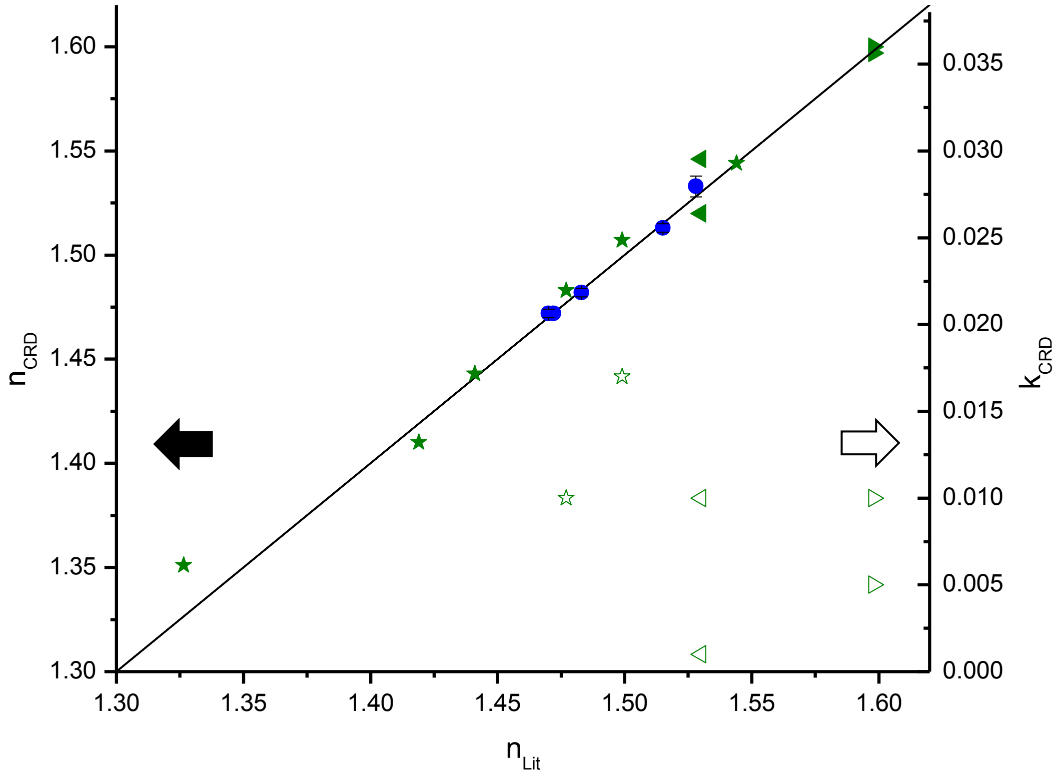

Figure 3.1 Complex refractive indices of pure scattering compounds collected by cavity ring down spectroscopy compared to literature values for the complex refractive indices. Solid markers correspond to the left axis representing n values; empty markers correspond to the right axis representing k values. Blue dots represent refractive index at 355 nm presented in this work. Green markers represent measurements collected by others at 532 nm. Square markers represent nigrosin, left-facing triangles represent ammonium sulfate, right pointing arrows represent SRFA, stars represent other compounds.

An example of extinction cross section measurements for oleic acid is presented in Figure 3.2. The calibration factors applied to this data are $C_f = 1.042$ and $\Delta d = +26$nm. The best fit complex refractive index for this data was 1.482 + 0.000i, represented by the solid black line, in close agreement with the Snell's Law measurement, 1.483 + 0.000i. The error bars on each extinction cross section represent the 68 percent confidence interval (CI) determined by $CI = \frac{\sigma}{\sqrt{N}}$ where the standard deviation, σ, was recorded in real time for each measurement and N represents the number of data points for each selected diameter. The error bars presented here demonstrate that the uncertainty on each cross section measurement is less than 2%. This precision improves the sensitivity to small changes in the complex refractive index, most specifically to small changes in k. The dashed line represents the Mie curve for the complex refractive index 1.487 + 0.010i, and is meant to simulate the false absorption commonly reported in the literature. In this case the k value was fixed to 0.010 and a best-fit n was determined using the Mathematica reverse Mie fit program. The difference between the 1.482 + 0.000i curve and the 1.487 + 0.010i curve differ by no more than 3%, highlighting the need for the high level of precision in measured extinction cross sections, which is demonstrated by the presented OA data.

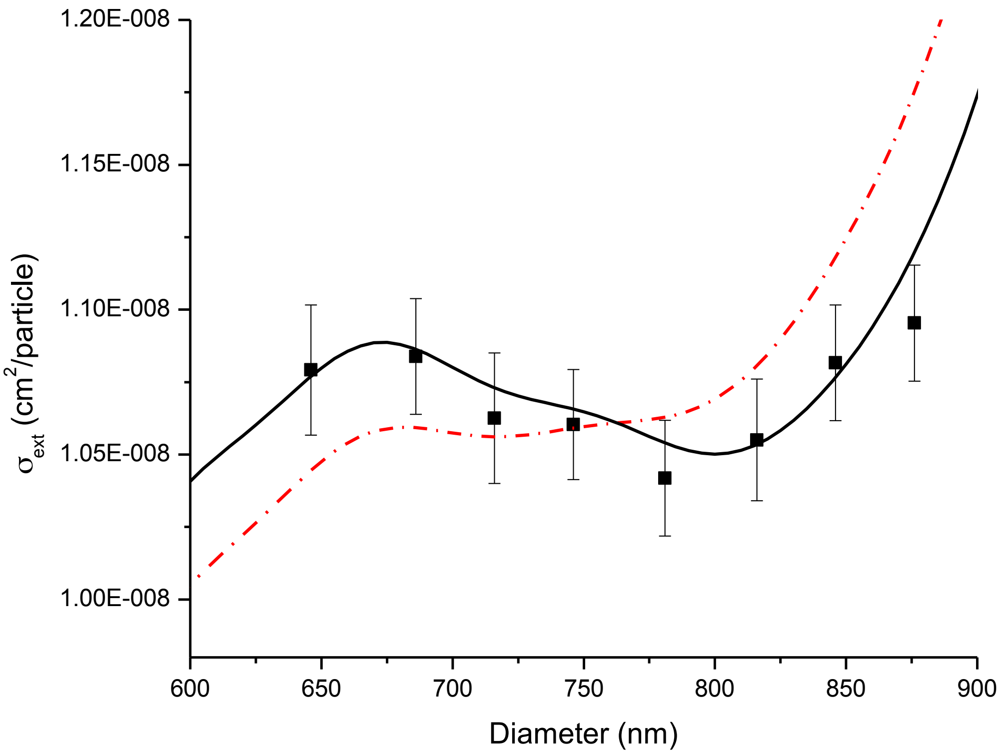

Figure 3.2 Oleic acid extinction cross section measurements fit to 1.483 + 0.000i. The squalane calibration factors applied are C_f = 1.002 and Δd = + 17 nm. The solid black line represents the 1.483 + 0.000i best fit, and the red dashed line is 1.487 + 0.010i representing the magnitude of false absorption sometimes reported in the literature.

Scattering Aerosols in Literature

Several studies use cavity ring down spectroscopy at 532 nm to measure the complex refractive index of ammonium sulfate, polystyrene latex spheres, PSLs, organic acids, and some salts. The results of these studies are presented in Figure 3.1 represented by green markers. The left-facing triangles represent reported refractive indices for ammonium sulfate with a range of 1.520 + 0.010i[29] to 1.546 + 0.00i, fit with a fixed absorption of k = 0.000.[30] Ammonium sulfate is a common validation compound used in CRD studies, despite this there remains a wide range of reported n values in the literature ± 0.013. Pettersson et al. claim to have used ammonium sulfate to calibrate their CRD instrument. In the same study they reported the complex refractive index of DOS at 532 nm as 1.455+0.003i[37] compared to 1.451+0.00i measured in this work using bulk techniques. PSLs are another common validation compound. Lang-Yona et al. reported the complex refractive index of PSLs at 532 nm as 1.598 + 0.010i.[29] Like ammonium sulfate, PSLs are pure scatterers at 532 nm. While the reported n value is in close agreement with the literature, 1.598 + 0.00i,[37] a 0.010 imaginary part was fit. A k value of 0.010 is equivalent to the absorption exhibited by a particle of the same size containing just 2% black carbon.[56]

The empty markers in Figure 3.1 represent the false absorption, k, values reported in the literature. A majority of the solid markers, representing n values, lie close to the 1:1 diagonal indicating accuracy in retrieving scattering measurements. Presence of empty markers for measurements where k should be 0.000 indicates measurements that are insensitive to small differences in extinction cross section. Not all groups allow the imaginary part of the complex refractive index to float when fitting complex refractive indices. Freedman et al. fixes k at zero before fitting a refractive index to collected measurements. In a study measuring salts and organic acids, Freedman et al. reported a refractive index of sodium fluoride as 1.351,[30] compared to the literature value of 1.327.[60] Accuracy of the real part could have been improved had the k value not been fixed, but then a false absorption would be reported.

The range of values reported in cavity ring down literature and the frequency of false absorption supports the notion that CRD instruments need careful calibration in order to achieve the sensitivity necessary to improve these fits. Uncertainties like false absorption could substantially skew the understanding of aerosols' contributions to the climate system. Most importantly, false absorption values as low as 0.01i dampen the radiative forcing efficiency of scattering particles by as much as 25%.[56]

3.3 Scattering Internal Mixtures

In order to demonstrate the applicability of the cavity ring down spectrometer to ambient aerosols, a 2:1 mixture of two well-studied compounds, squalane and squalene, was measured. Squalane and squalene have known complex refractive indices at 355nm of 1.472 + 0.000i and 1.530 + 0.000i. As described in the previous section, the refractive indices of these compounds have been measured using CRDS as well as several bulk techniques. The volume fraction mixing rule was used to predict the expected complex refractive index for these binary particles.

The volume fraction mixing rule describes the contribution of each component in a mixture to the overall optical properties based on their volume fractions, *f*. In this case, the linear mixing rule is used for the prediction of an effective real part of the complex refractive index, n_{eff}, based on the refractive indices of the two components, n_1 and n_2.

$$n_{eff} = f_1 n_1 + f_2 n_2 \tag{1}$$

The volume fraction mixing rule predicts $n_{eff} = 1.491$ for a 2:1 squalane:squalene mixture. The volume fraction mixing rule can also be used to predict the imaginary part of the complex refractive index. Both squalane and squalene are pure scatterers in the UV-Visible region so the predicted $k_{eff} = 0.000$.

The literature cites several mixing rules for the prediction of complex refractive indices in mixed aerosols particles, but the volume fraction mixing rule is most common.[30,34,39] Predictions using alternative mixing rules, including the Maxwell-Garnett and the effective dielectric medium approximations, were nearly identical to the linear mixing rule.[34] Due to its simplicity and accuracy, all predicted refractive indices presented here were calculated using the volume fraction mixing rule.

Complex Refractive Indices of Scattering Internal Mixtures

The measured complex refractive indices for the 2:1 squalane:squalene mixture averaged to 1.490 + 0.000i, in close agreement with the predicted 1.491 + 0.000i. The specific results are presented in Table 3.1. The close agreement between the predicted and reported complex refractive indices demonstrates that the volume fraction mixing rule accurately predicts the effective complex refractive index for binary mixtures in aerosols. All mixtures included in Table 3.1 are pure scatterers in the UV-Visibile region. Unlike the values reported in the literature, none of the refractive indices for this work were fit to false absorbing components. Additionally, Table 3.1 illustrates how tightly clustered the best-fit refractive index values are. The error bars reported for these measurements were all less than 0.001 and therefore appear in Table 3.1 as 0.000. These small error bars are an artifact of large best-fit χ_0^2 values, all were between 20-50. Best fit χ_0^2 of this magnitude will limit the number of refractive indices within the 68 percent confidence interval.

Table 3.1 Aerosol binary mixture complex refractive indices. All complex refractive indices presented by Riziq et al. and Freedman et al. were collected at 532 nm, complex refractive indices from this work were collected at 355 nm.

Mixture	Mixing Rule n	Mixing Rule ik	CRDS n	CRDS ik	Source
1:1 NaCl:Glutaric Acid	1.477	0.00i	1.483	0.01	Riziq et al.2007[34]
2:1 NaCl:Glutaric Acid	1.499	0.00i	1.507	0.017	Riziq et al.2007[34]
3:1 Succinic Acid : $(NH_4)_2SO_4$	1.49	0.00i	1.589	0.00	Freedman et al. 2009[30]
2:1 Squalane:Squalene	1.491	0.000i	$1.488\,(^{+0.000}_{-0.000})$ $1.488\,(^{+0.001}_{-0.000})$ $1.501\,(^{+0.001}_{-0.000})$ $1.484\,(^{+0.001}_{-0.000})$	$0.000\,(^{+0.000}_{-0.000})$ $0.000\,(^{+0.001}_{-0.000})$ $0.001\,(^{+0.000}_{-0.001})$ $0.000\,(^{+0.001}_{-0.000})$	This work

Scattering Internal Mixtures in the Literature

A study of aerosol mixture by Freedman et al. measured a 3:1 succinic acid:ammonium sulfate mixture yielding a complex refractive index of 1.589 compared to the predicted 1.491.[30] In this case the Mie fit was conducted with a fixed absorption of k = 0. If the real part of the refractive index were fixed to 1.490 Freedman et al. state that the absorption value would need to be k = 0.59 in order for the theoretical and measured extinction cross sections to agree.[30] Similar experiments performed by Riziq et al. using CRDS for the measurement of scattering mixtures have reported false absorption as large as 0.017i.[34] This absorption measurement was fit to a scattering mixture of 2:1 sodium chloride:glutaric acid. The refractive index reported was 1.507 + 0.017i, compared to the predicted 1.499 + 0.000i. Similarly the complex refractive index reported for a 1:1 mixture was 1.483 + 0.010i.[34] Riziq et al. attributed the false absorptions reported to the particle sizes measured, indicating that there is a minimal difference between the absorbing and non-absorbing extinction cross sections at the sizes selected. Riziq et al. went on to explain that the sizes selected for the experiment were chosen based on their atmospheric relevance.[34] The false absorption reported by Riziq et al. is larger than the direct absorption measurement reported by Lack et al. for ambient particles, k = 0.007.[22] The sizes used in Riziq et al. range from 100 to 600 nm, a region of the curve with minimal sensitivity to small changes in the refractive index. Measurement reported in this work were collected between 600 and 900 nm, a region where, as demonstrated by Figure 3.2, there is a 3% difference between the absorbing and pure scattering Mie curves.

3.4 Absorbing Internal Mixtures

The previous section demonstrated the validity of the linear mixing rule for the prediction of the real part of the refractive index. In this section the linear mixing rule is used to predict the imaginary part of the complex refractive index for a binary absorbing aerosol mixture. The absorber used was 2-(2-benzotriazol-2-yl)-6-dodecyl-4-methylphenol (BDMP) which, as shown in Figure 3.3, is a strong UV absorber making it a good model for absorbing ambient aerosol. BDMP has a strong absorption at 355 nm making it an attractive compound for these experiments. It also serves as a good model for organic carbon aerosols because its absorption spectrum drops off abruptly at 400 nm.

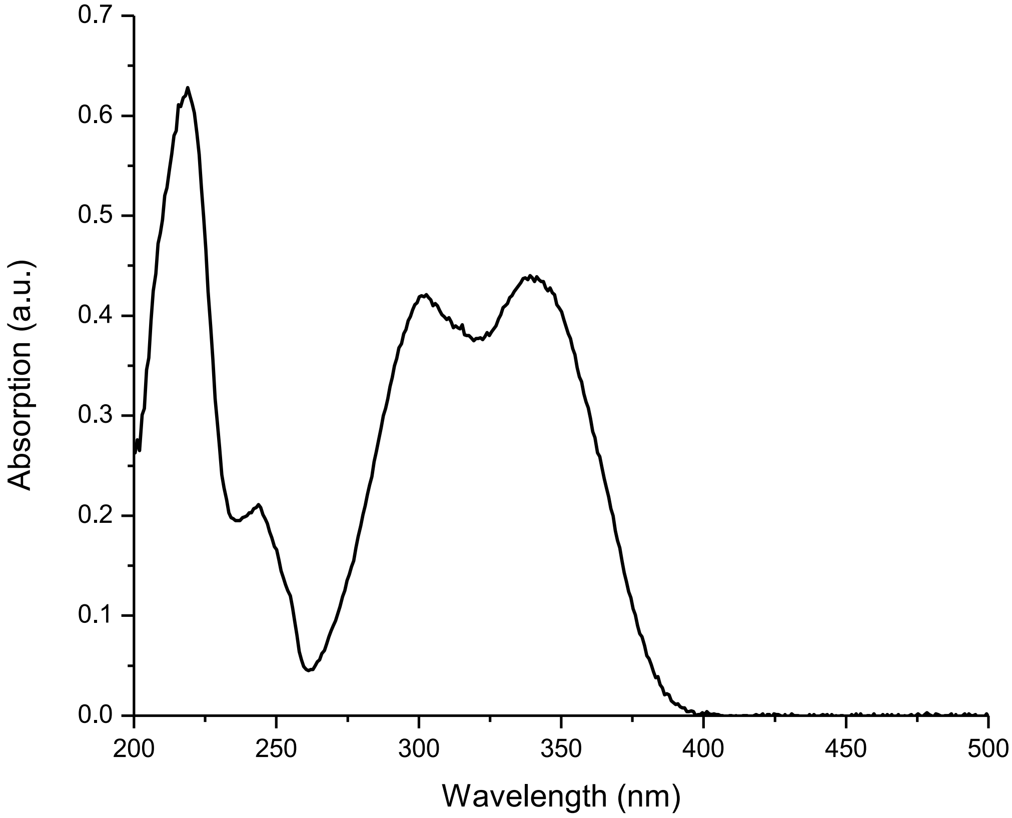

Figure 3.3 UV Visible absorption spectrum of BDMP, which is a strong absorber in the UV region but tails off quickly near 400 nm making it a good model for absorbing atmospheric aerosols.

Similar to the binary mixture described in the previous section, BDMP was mixed with squalane. The refractive index of BDMP at 355nm is not available in the literature. Due to the viscosity, BDMP could not be nebulized as a pure compound, and therefore a refractive index could not be determined via CRDS. Without a reference refractive index for BDMP the linear mixing rule cannot be used to predict the effective complex refractive index for the mixture. However, the molar absorptivity can be used in order to determine a bulk imaginary part for BDMP, which can then be used in the volume fraction mixing rule. According the equation below, a bulk k_{BDMP} value can be calculated at a known wavelength, λ, using the molar absorptivity, ε,

$$k_{BDMP} = \frac{1000 \ln 10 \cdot \rho \cdot \lambda \cdot \varepsilon}{4\pi MW} \tag{2}$$

where MW is molecular weight and ϱ is density.[12] This calculation yields a bulk value of $k_{BDMP} = 0.19$. Using the bulk k_{BDMP}, the linear mixing rule can then be used to predict a k_{eff} based on the volume fraction of BDMP and squalane, f_{BDMP} and f_{sqa}.

$$k_{eff} = f_{sqa} k_{sqa} + f_{BDMP} k_{BDMP} \tag{3}$$

The refractive index of squalane is 1.472+0.000i, therefore k_{eff} is only dependent on the volume fraction of BDMP, f_{BDMP}. In these experiments the refractive indices were measured for five BDMP:squalane mixtures ranging from 2% to 15% by volume.

Generating the Absorbing Mixtures

A known mass of BDMP, dependent on the desired volume fraction, was added to a 25.00 mL volumetric flask. The remaining volume was filled with squalane. The solution was set in a dark place, to prevent degradation, and mixed overnight. Aerosols measured in CRD experiments were generated directly from this volumetric flask. The exactly volume fraction of BDMP was determined for each mixture and input into the volume fraction mixing rule in order to predict k_{eff}.

Measured Complex Refractive Indices

The results displayed in Figure 3.4 show close agreement between the predicted and measured k for all five BDMP:squalane mixtures. BDMP:squalane mixtures serve as a good model for weakly absorbing organic carbon aerosols. The typical absorption range of ambient aerosols is k = 0.01 – 0.71.[23] These measurements are more relevant to ambient aerosols than other absorbers found in the literature, namely nigrosin, k =0.26,[57] or SRFA, k = 0.02[29] at 532 nm.

The volume fraction mixing rule predicted an absorption of $k_{predicted} = 0.028$ for the most concentrated of these mixtures, 15% BDMP in squalane. The point appearing at $k_{CRD} = 0.034$ is notably higher than the other tightly clustered points measured for the 15% mixture. This particular data point is associated with a calibration that returned typical C_f and Δd value, 0.996 and 16 nm, but had a χ^2 value two orders of magnitude larger than other calibrations indicating that the squalane calibration was not very good. Additionally, the real part associated with this k value, n = 1.493, is much lower than others reported for the same 15% mixture, typically n = 1.505. The large χ^2 associated with the calibration and systematically high absorbing part of the complex refractive index suggests an error not accounted for by the calibration factors, C_f and Δd. Despite the large χ^2 the extinction cross sections associated with $k_{CRD} = 0.035$ point are within 14 percent of the extinction cross sections predicted by Mie theory.

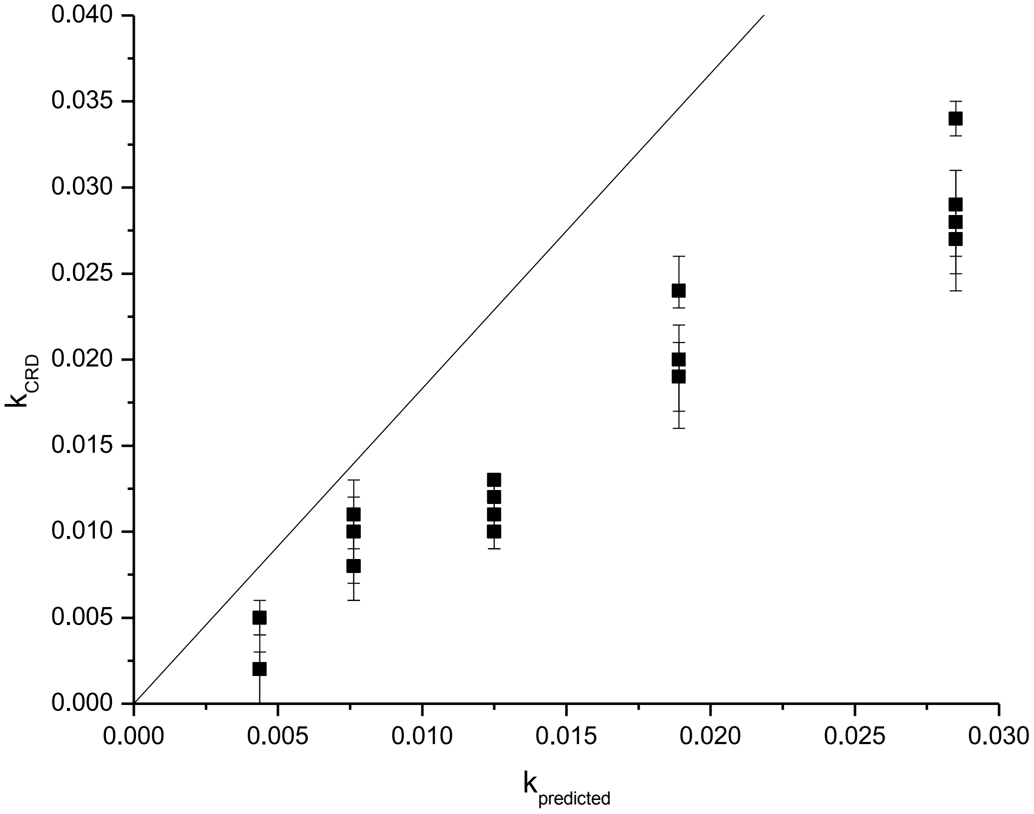

Figure 3.4 Comparison of linear mixing rule predicted k values for BDMP:squalane to CRDS measured k values. Error bars reported on these measurements range from ±0.000-0.003.

The least concentrated mixture, 2% BDMP, fit a refractive index range of 1.472 + 0.002i to 1.477 + 0.005i in close agreement with the predicted k = 0.004. To our knowledge this is the smallest absorption measurement of an absorbing aerosol mixture using CRDS. Figure 3.5 shows data collected for the 2% BDMP:squalane mixture adjusted to C_f = 1.002 and Δd = +17 nm. The solid black line represents the best-fit complex refractive index of 1.476 + 0.005i. The dashed red lines represent complex refractive indices fit to extinction cross sections at the boundary of the 68 percent confidence interval. The effective extinction cross sections presented in this figure demonstrates our ability to discern between small absorptions.

The region between 600 and 900 nm is the region of the Mie curve were extinction cross sections are most dependent on diameter allowing discernment between k = 0.005 and k = 0.000. Riziq et al. indicated that the error reported in their mixture experiments could be attributed to the sizes selected in their experiment. The sizes selected in their study were between 100 and 600 nm.[34] All curves presented in Figure 3.5 converge below 580 nm limiting the sensitivity to small changes in n or k values. The effect would be similar for complex refractive indices reported at 532 nm. The Mie curve is wavelength dependent and will appear slightly different at 532 nm but the lack of sensitivity at small sizes is the same.

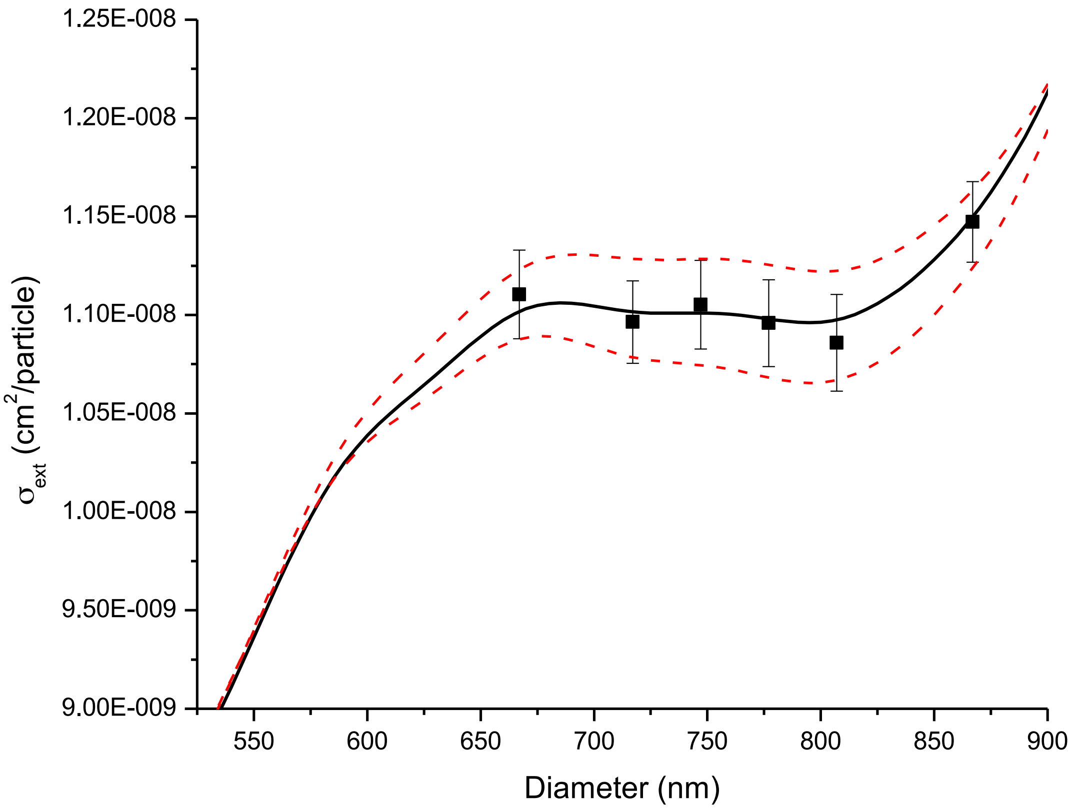

Figure 3.5 Extinction cross section measurements for 2% BDMP:squalane compared to the best fit complex refractive index 1.483 + 005i, represented by the solid line. The dashed lines represent the 68th confidence interval, the upper bound is 1.476 + 0.006i and the lower bound is 1.481 + 0.000i.

Absorbing Aerosol Mixtures in the Literature

As discussed in the previous section, there are few CRD measurements in the range of weakly absorbing ambient aerosols. One study from Riziq et al. used a mixture of rhodamine 590 (Rh-590), an absorbing dye, and ammonium sulfate (AS), as a model for these weakly absorbing particles. This study measured several mixtures ranging from 1:10 Rh-590:AS to 1:500 Rh-590:AS. The expected k values were predicted using the volume fraction mixing rule. Results are compared to predicted values in Figure 3.6 represented as green squares.

The predicted complex refractive index for the most dilute Rh-590:AS mixture, 1:500, was 1.516 + 0.008i. The measured complex refractive index, however, was 1.526 + 0.103i.[34] The reported absorption was 13x larger than the 0.008 predicted by the mixing rule. An error of this magnitude could indicate that the volume fraction mixing rule cannot predict accurate k values for this mixture. Riziq et al. compared the retrieved result to alternative mixing rules, including Maxwell-Garnett and effective dielectric medium approximations, but all mixing rules predicted absorption between k = 0.008 and k = 0.013.[34] The accuracy of retrieved complex refractive indices reported in this study did not improve with concentration. The most concentrated solution, 1:10 Rh-590:AS, was reported to have a complex refractive index of 1.405 + 0.486i, 2x more absorbing than the predicted 1.416 + 0.205i.[34]

Figure 3.6 displays the reported absorption values for the Rh-590:AS mixtures. As described above these reported k values do not agree with those predicted by any of the mixing rules tested. Also presented in Figure 3.6 are absorption measurements for nigrosin, near $k_{pred} = 0.26$, and SRFA, near $k_{pred} = 0.02$. Both show close agreement with the k values measured by alternate absorption measurement techniques.[19,21] The range of absorption values reported by other studies for both SRFA and nigrosin is within ±0.003 of the values displayed in Figure 3.6 demonstrating the reproducibility of moderate to strong absorption measurements.[18,19,28,29] In an ambient measurement study, Dinar et al. reported complex refractive indices for pollution, 1.595 + 0.049i, and smoke, 1.622 + 0.049i.[18] These absorption values lie between the absorption values reported for nigrosin and SRFA, support the use of CRDS as an accurate technique for the measurement of strong ambient absorption. However, studies reporting absorption measurements 13x larger than the predicted, like the study of Rh-590:AS mixtures, demonstrate the need for additional work focused on weakly absorbing aerosol particles.

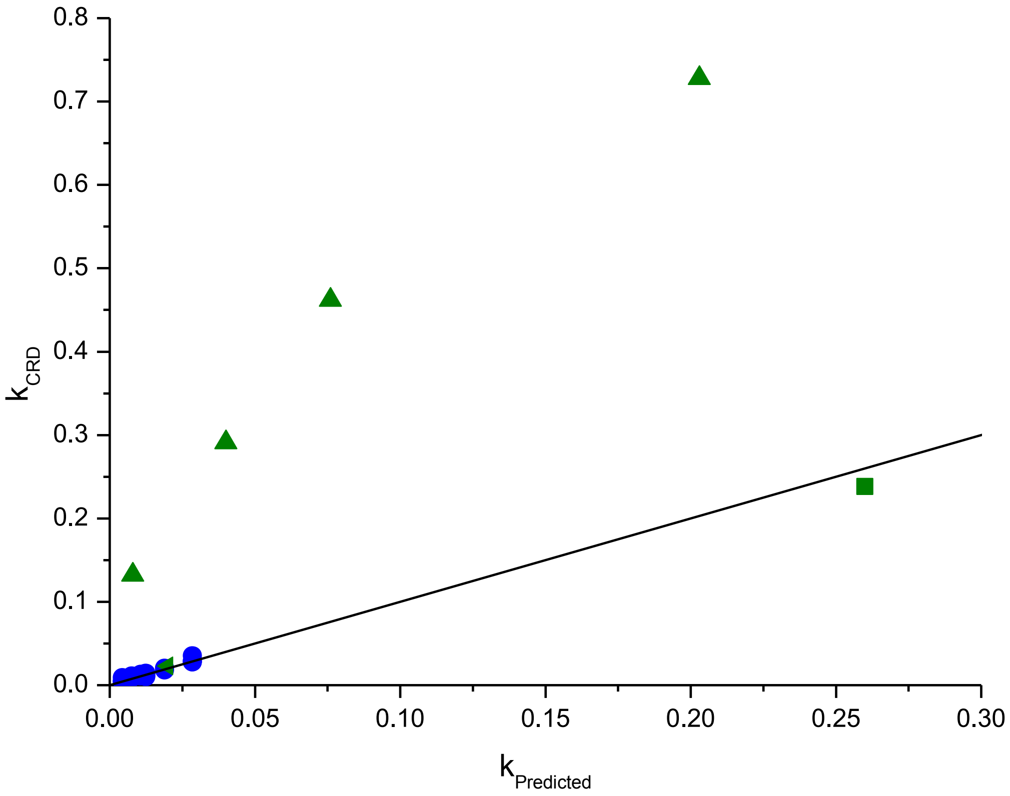

Figure 3.6 Comparison of literature k and CRD k values for both single component and binary mixture absorbing aerosols at 355 nm and 532 nm. Blue dots represent BDMP:squalane mixtures at 355 nm. Green markers indicate measurements collected at 532 nm. Triangle markers represent Rh-590:AS mixtures. Square markers represent nigrosin and left facing triangles represent SRFA.

3.5 Conclusions

The complex refractive indices presented in this chapter illustrate the accuracy of the calibrated cavity ring down system for the measurement of atmospherically relevant weakly absorbing aerosols. Many studies discussed report false absorptions for purely scattering compounds as large as k = 0.017.[34] Erlick at al. demonstrated that a false absorption of k = 0.01 is equivalent to an aerosol particle containing just 2% black carbon. A particle with this absorption will exhibit a radiative forcing efficiency 25% smaller than a pure scattering particle in the same conditions.[56] This 25% could have a serious impact on the Earth's radiative balance. Lang-Yona et al. reported the complex refractive index of purely-scattering ammonium sulfate as 1.52 + 0.01i.[29] Accurate measurement of this compound is of particular importance because it is a naturally occurring aerosols and frequently appears in climate model studies.[2,11] Misrepresentation of this compound will lower the radiative forcing efficiency from -26.33 W/m^2 to -19.20 W/m^2.[56]

The scattering compounds and mixtures presented in this work report the real and imaginary parts of the complex refractive index within ± 0.002 of the literature values. None of the compounds measured were fit to false absorption components demonstrating our sensitivity to small changes in extinction cross sections. This high level of accuracy can be attributed to the squalane calibration applied to each measurement. By accounting for day to day changes in the CRD system the percent error between predicted and measured extinction cross sections is minimized improving the overall Mie fit. Complex refractive indices reported for DOS, OA, and squalene were in close agreement with the bulk measurements presented in Table 2.1. This type of external validation is unique to this work; CRD studies in the literature have limited reference because compounds like PSLs must be aerosolized for measurement.

Complex refractive indices for the scattering mixtures studied here are in close agreement with the volume fraction mixing rule. This mixing rule predicts the effective complex refractive index for an aerosol based on the proportions of the components. In this case a pure scattering mixture of squalane:squalene was reported to have an average complex refractive index of 1.490 + 0.000i, in close agreement with the predicted. The error on these measurements was less than ± 0.001 for both n and k values validating the application of the volume fraction mixing rule to aerosol particles. Mixture studies in the literature reported complex refractive indices for pure scattering mixtures with k values ranging from 0.01 to 0.017.[34]

The BDMP:squalane mixtures presented here serve as a good model for absorbing organic carbon particles. The wavelength dependent absorption of BDMP drops off sharply at 400 nm. Kirchstetter et al. indicate that the k value for organic carbon decreases from k = 0.168 to k = 0.030 between 350 nm and 550 nm. The complex refractive indices reported for the BDMP:squalane mixture range from $1.474\left(^{+0.002}_{-0.001}\right) + 0.004i\left(^{+0.001}_{-0.002}\right)$ to $1.505\left(^{+0.003}_{-0.001}\right) + 0.028i\left(^{+0.002}_{-0.003}\right)$. The error on each measurement is less than two percent of the overall extinction demonstrating a sensitivity of the calibrated CRD not demonstrated previously in the literature. This type of sensitivity allows for atmospherically relevant weak absorption to be measured.

There are several examples in the literature of strong absorption measurements in an atmospherically relevant range. Nigrosin and SRFA have complex refractive indices of 1.67 + 0.26i[57] and 1.65 0.02i[29], on the same order of magnitude as black carbon, k = 0.71.[58] Dinar et al. reported the complex refractive index of smoke and pollution aerosols as 1.622 + 0.049i and 1.595 + 0.049i,[18] these absorptions lie between nigrosin and SRFA. Kirchstetter et al. indicate that smoke particles are primarily made up of black carbon while particles generated by pollution or biomass burning may contain organic carbon. The organic carbon component does not contribute as much to the overall extinction measured in the visible, but in the UV organic carbon significantly enhances the absorption effect.[58] There are few examples in the literature of accurate measurements of organic carbon aerosol absorption, and the BDMP:squalane mixtures presented here serve as an accurate model for these particles.

CHAPTER 4

COMPLEX REFRACTIVE INDEX MEASUREMENTS OF EXTERNALLY MIXED AEROSOLS USING A CALIBRATED CAVITY RING DOWN SPECTROMETER

4.1 Introduction

In contrast to the internal mixtures presented previously, this chapter discusses measurement of external mixtures of single component aerosol particles. These mixtures can be thought of as many single component particles occupying one cubic meter of the atmosphere. Ambient external mixtures are often a collection of aerosols from many sources. The mixing state of aerosol particles greatly impacts their optical properties. Black carbon particles for instance, exhibit an absorption enhancement effect when coated, internally mixed, with organic compounds.[22,39,61] All ambient aerosol samples are external mixtures; no two particles are exactly alike. In one sample there may be many internally mixed particles, many different single component aerosols, or some variation thereof. No matter the makeup of the aerosols, the mixing state of the total ensemble is important to the overall optical properties. Presented here is a size selected 1:1 mixture of squalane and squalene particles as well as a squalene external mixture consisting of pure particles of varied charge states.

4.2 Squalane : Squalene External Mixtures

The squalane:squalene external mixture demonstrates the importance of mixing state in the accurate retrieval of complex refractive indices. Assuming particles are internally mixed, and therefore using the volume fraction mixing rule, may lead to an incorrect prediction of the complex refractive index. An alternative technique presented in a study by Dinar et al. is to select for the mixing state. In this study ambient aerosols were trapped on a filter and re-aerosolized for measurement by CRDS. Through this process Dinar et al. was able to size select particles and report a complex refractive index.[18] Measuring the complex refractive index in this way may underestimate the extinction observed for particle in their natural state. In order to avoid this type of biased result, many *in situ* measurement of external mixture employ a secondary measurement technique to directly measure the absorption observed in an ambient aerosol sample.[62,63]

This section demonstrates the importance mixing state in the accurate prediction of the complex refractive index for a 1:1 squalane:squalene external mixture. Utilizing the volume fraction mixing rule, therefore mimicking an internal mixture, each component should contribute equally to scattering and absorbing components of the complex refractive index, predicting 1.5000 + 0.000i. If, however, a complex refractive index is fit to the average of the extinction cross sections for squalane and squalene particles, simulating an external mixture, the predicted complex refractive index is 1.500 + 0.0006i. Both squalane and squalene are purely scattering in the UV, however, the averages of the extinction cross sections demonstrates a rapid increase in extinction at larger particle sizes.

In order to measure the extinction of a 1:1 squalane:squalene external mixture directly, particles are generated and size selected independently before mixing and flowing into the CRD cell. Size selecting in this manner allowed a complex refractive index to be fit to the measured extinction cross sections. Concentrations of squalane and squalene are carefully controlled to ensure a 1:1 mixture is achieved. Assuming a perfect 1:1 mixture each component should contribute equally to the measured extinction cross sections.

Generating a 1:1 External Mixture

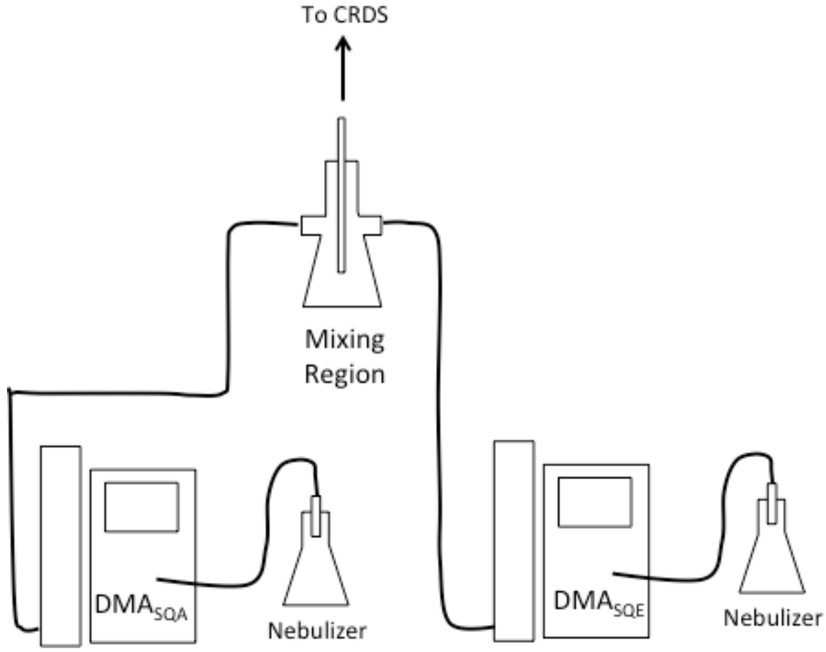

Figure 4.1 Instrument diagram for particle generation and size selection of a 1:1 squalane:squalene mixture.

Generating Size Selected External Mixtures

Two particle sources were used in order to generate and size select squalane and squalene particles, Figure 4.1. Particles were generated from a reservoir of compound using a concentric nebulizer, and the particles were then size selected using separate differential mobility analyzers (DMA). Particle concentrations were carefully monitored in order to prevent particle aggregation and to ensure a 1:1 mixture was achieved.

Particle Size Selection

Both squalane and squalene particles were size selected with independent DMAs. In order to determine the diameter offset between DMA_{SQA} and DMA_{SQE}, particles were size selected with DMA_{SQA} and flowed into DMA_{SQE}. Diameters were then scanned by DMA_{SQE}, and the resulting maximum concentration indicated the relative offset between the two DMAs. The typical offset was +15 nm. As a result, DMA_{SQE} was set to size select particle diameters 15 nm smaller than DMA_{SQA}. This offset is a remnant of the DMA-specific Δd shift described in Chapter 2.

Calculation of Extinction Cross Sections

Once size selected, particles were flowed into a mixing flask before entering the CRD cell where they interacted with 355 nm radiation. Finally particles flowed into a concentration particle counter (CPC), where a number density was reported. A custom LabVIEW program calculated the extinction cross sections in real time using the total extinction measured and the number density reported by the CPC. For each diameter of interest, three extinction cross sections were recorded: first for squalane, then the external mixture, and finally squalene. In order to perform these measurements the CRD cell was filled with squalane particles. Then squalene was flowed into the cell and the concentration was adjusted until the CPC reported a number density 2x the original squalane concentrations. Finally squalane was removed and only squalene was left in the cell.

A custom reverse Mie fit Mathematica program determined the best fit complex refractive index using the measured extinction cross sections at the given diameters. A complex refractive index was fit to all three ensembles measured, squalane, the external mixture, and squalene. The best-fit value is associated with the complex refractive index returned the lowest χ^2, defined by $\chi^2 = \sum_{i=1}^{N} \frac{(\sigma_{ext} - \sigma_{Mie})_i^2}{\varepsilon_i^2}$, where σ_{ext} and σ_{Mie} represent the extinction cross secton measured with CRD and predicted by Mie theory, and ε represents the variance.

External Mixtures

Chapter two demonstrated the accuracy of the volume fraction mixing rule for the prediction of complex refractive indices for internal mixtures. This is a powerful prediction technique when the mixing state of the aerosol is known. If, however, the aerosol is an external mixture the volume fraction mixing rule will not accurately predict the complex refractive index. In instances where the mixing state is unknown, like ambient aerosol mixtures, this is an important issue. The extinction cross section curves presented in Figure 4.2 demonstrate the difference between the complex refractive index predicted by the volume fraction mixing rule, solid black line, versus the average of contributing extinction cross sections, dashed black line.

For a 1:1 squalane:squalene mixture the volume fraction mixing rule predicts a complex refractive index of 1.500 + 0.000i, represented by the solid black line. The average of the extinction cross sections, represented by the dashed black line, does not lie along this curve; instead it corresponds to a best fit complex refractive index of 1.500 + 0.006i. Squalane and squalene are purely scattering compounds in the UV meaning that any absorption predicted in this theoretical calculation must be an artifact of the fitting procedure. Over the measurement region the percent difference between 1.500 + 0.000i and 1.500 + 0.006i is less than 2.5%. Chapter 3 demonstrated the uncertainty of the calibrated CRD is as low as 2% and the smallest BDMP:squalane absorption measured was k = 0.004i, indicating that under ideal circumstances the CRD may be sensitive enough to measure this difference.

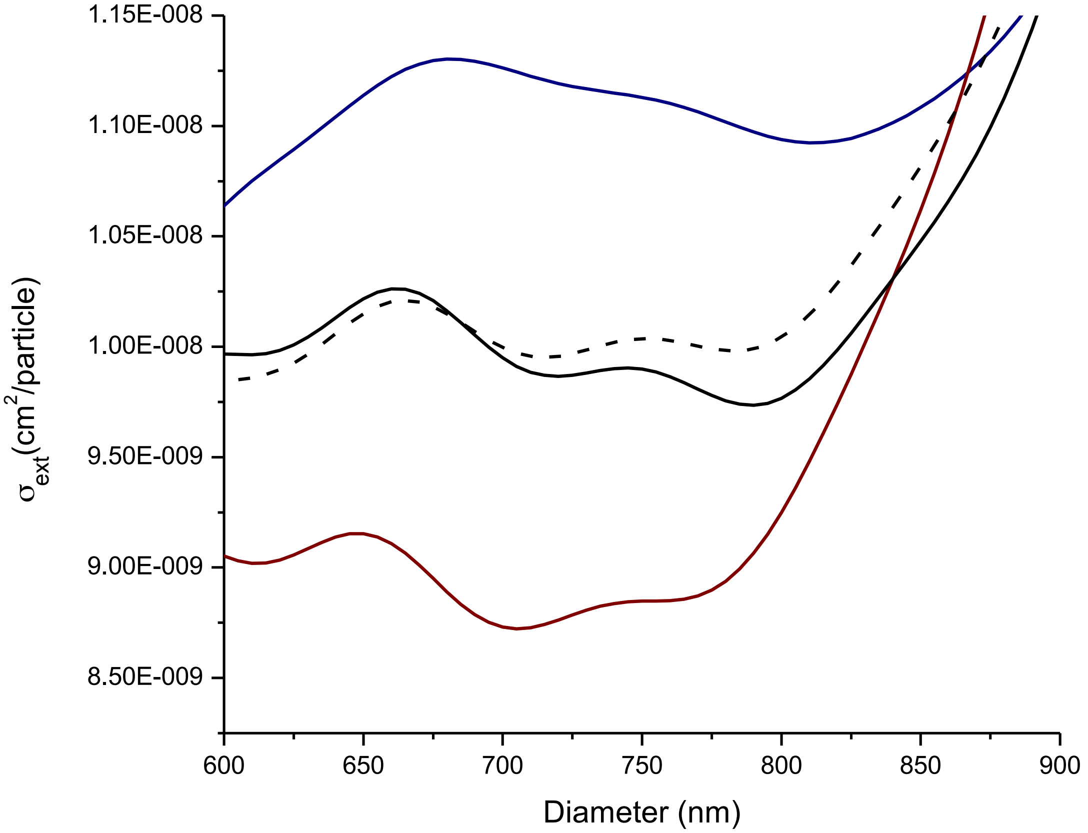

Figure 4.2 Theoretical extinction cross section curves corresponding to complex refractive indices of squalane, squalene, a 1:1 squalane:squalene external mixture. The solid black line represents the volume fraction mixing rule predicted complex refractive index 1.500 + 0.000i. The dashed black line represents the average 1:1 cross sections, best fit 1.500 + 0.006i. The blue solid line is squalane 1.472 + 0.000i and the red solid line is squalene1.530 + 0.000i.

Experimental results are represented in Figure 4.3 as square-black markers and compared to the theoretical curves. The results displayed represent diameters chosen ranging from 650 to 840 nm adjusted to $\Delta d = +22$ nm, associated with DMA_{SQA}, and $C_f = 0.940$. In this case all calibration factors were determined prior to collection of any external mixture data. The relative uncertainty on each extinction cross section measurement was less then 2%. The black markers representing the externally mixed aerosol fit more closely to the black dashed line than the solid black line, mimicking the small absorption, k =0.006. Deviations from this dashed line could be attributed to small uncertainties in the concentration of either component in the mixture. The dashed curve was generated assuming a perfect 1:1 mix of particles, and a small difference in either components concentration could affect the measured extinction cross section enough for the fitting routine to miss the small absorption. The smallest absorption measured in Chapter 3 was k = 0.004i, where this type of sensitivity was possible because any uncertainty in concentration was accounted for with C_f.

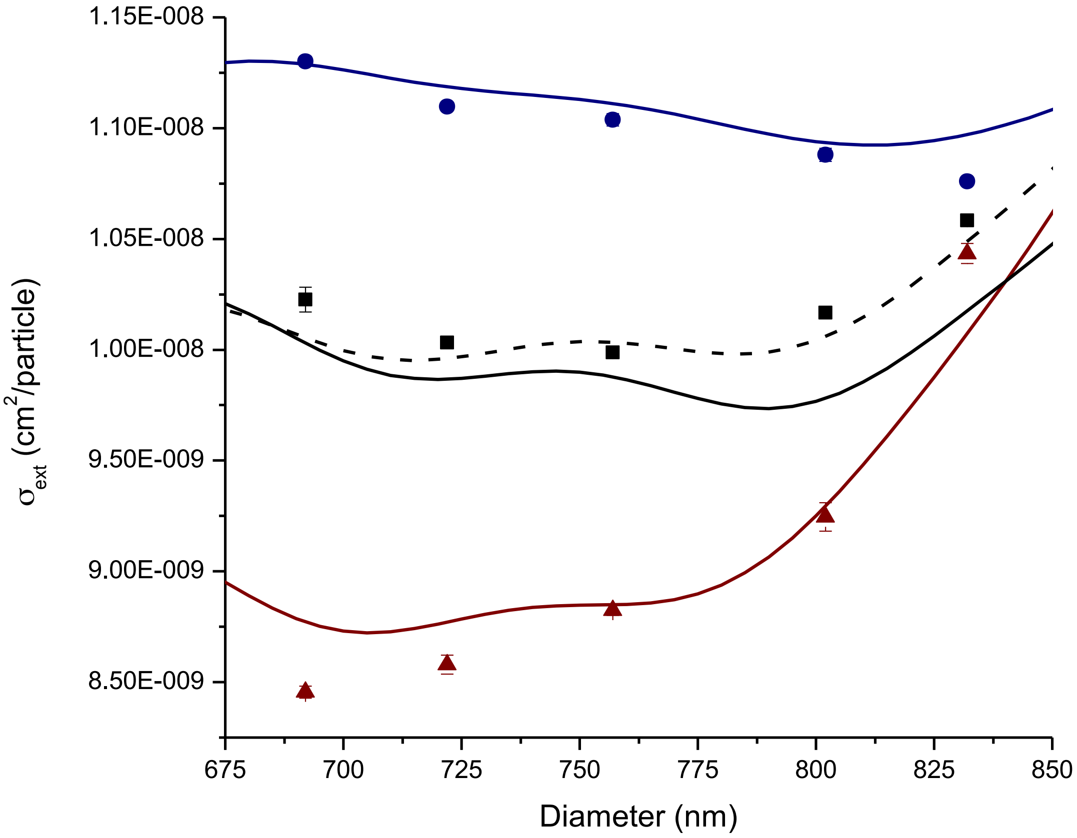

Figure 4.3 Extinction cross section of 1:1 Squalane:Squalene external mixture. The black markers and line represent extinction cross sections measured for the external mixture and the complex refractive index 1.500 + 0.000i corresponding to the volume fraction mixing rule prediction. The dashed black line represents 1.500 + 0.006i, the best fit refractive index for the ideal 1:1 external mixture. Blue circular markers represent squalane measurements and correspond to the blue line representing 1.472 + 0.000i. Red triangular markers represent squalene measurements and correspond to the red line representing 1.530 + 0.000i.

Mixing state plays an important role in the overall optical properties of an aerosol mixture. This importance is illustrated by the difference in complex refractive index between the volume fraction mixing rule and the averaged cross sections presented for the squalane:squalene external mixture. Measuring the absorption directly, however, would minimize the role of mixing state. Many studies that report complex refractive indices for ambient aerosol use a secondary method in order to determine the absorption component. There is a 2% difference between the extinction cross section predicted associated with the complex refractive index predicted using the volume fraction mixing rule, i.e. assuming an internal mixture, and the complex refractive assuming an ideal 1:1 external mixture. Despite this small difference the extinction cross sections measured for the external mixture were clearly in closer agreement with the 1.500 + 0.006i curve demonstrating the importance of mixing state.

External Mixtures in the Literature

There are several studies in the literature demonstrating a synergistic approach to complex refractive index measurements for external mixtures. A majority of these studies measure the absorption of ambient aerosol using a dedicated instrument. One study, conducted over Paris by Raut et al. demonstrated the use of Lidar, a sunphotometer, and an aethalometer for the measurement of ambient complex refractive indices.[17] The absorption component reported was measured by the aethalometer, an instrument that measures the concentration and absorption of black carbon. Including an external absorption measurement, like an aethalometer, ensures accuracy in the absorption component of the complex refractive index in addition to parameterizing the inversion of the Lidar data, thus avoiding the kind of error discussed in the previous section.

Another study conducted by Ebert et al. reported complex refractive indices for mineral dust in rural areas using a combination of total reflection X-ray fluorescence and high resolution scanning electron microscopy to analyze filter samples. In this study Ebert et al. utilized the total particle distribution and composition information in order to calculate the complex refractive index.[62] Like the previous study the multiple techniques were used in order to determine both the mixing state of the collected aerosol as well as the complex refractive index.

Alternatively, Dinar et al. captured and re-aerosolized ambient particles before using CRDS to measure the complex refractive index thereby selecting for the mixing state.[18] This method enabled Dinar et al. to size select aerosols and measure a complex refractive index but eliminated any mixing state specific optical properties. The black curves in Figure 4.2 illustrate the difference in extinction between internal and external mixtures. Dinar et al. may be losing extinction information at large particle sizes following this technique.

4.3 Multiple-Charged Particles

Multiple-charged particles are a common problem when size selecting small particle using a DMA. When aerosols enter the DMA they are passed through a radioactive krypton source where a uniform charge distribution is applied. Particles are then selected based on their differential mobility in the selection region. This region is made up of a grounded outer wall and an electrified inner rod. The current applied to this inner rod is dependent on the particle diameter of interest. Particles that are too large will be lost to the outer wall while particles that are too small will be pulled to the inner rod and lost. Those particles of the desired diameter will pass through the selection region unchanged. This is a simple enough concept in the diameter range of 600 to 900 nm, the size range where most measurements here are collected because the inertial impactor at the inlet of the DMA removes most of the larger particles that would be doubly charged. However, when selecting particles smaller than 580 nm the incidence of multiply charged particles is no longer negligible. When selecting for 580 nm particles the central rod is charged to allow singly charged particles of 580 nm to pass. A doubly charged particle of 950 nm will also pass through the selection region. These two particles exhibit a similar electric mobility despite the difference in size. For diameters smaller than 300 nm both doubly and triply charged particles must be accounted for.

The incidence of these multiply-charged large diameter particles can be attributed to the distribution of the particle source, in this case a concentric nebulizer. The concentric nebulizer used to generate the aerosol particles in these experiments produces a log normal distribution centered at a geometric mean of 400 nm. Many CRDS studies in the literature use an atomizer to generate particles within the 100 – 600 nm size range. The output distribution of the atomizer is centered at a much smaller diameter, typically around 200 nm, limiting the occurrence of large diameter particles. Working in this region, however, limits the efficiency of the inertial impactor, transmitting the full distribution and increasing the occurrence of doubly and triply charged particles in the output of the DMA.

The inclusion of multiply charged particles will overestimate the extinction cross section for a select diameter, in turn affecting the resulting complex refractive index. Multiply-charged particles have a larger diameter meaning they absorb and scatter light more efficiently. Hasenkopf et al. propose a correction factor to account for multiply charged particle contribution to the extinction cross section.[64] Few studies in the literature, however, have measured the contribution of multiply-charged particles to measured extinction cross sections. Measurements presented in this section demonstrate the sensitivity of our CRDS to changes in extinction cross section measurements due to contributions by multiply-charged particles from 320 – 900 nm.

Measuring Multiple-Charge Contribution

Figure 4.4 presents extinction cross sections for squalene measured between 380 and 900 nm adjusted in this case to $C_f = 0.978$ and $\Delta d = + 20$ nm. For diameters larger than 550 nm the measured extinction cross sections lie close to the solid black curve representing the complex refractive index of squalene, 1.530 + 0.000i. At smaller sizes less than 550 nm, however, the contribution of doubly- and triply-charged particles is apparent. A complex refractive index was fit to the full range of sizes resulting in a best fit complex refractive index of 1.527 + 0.000i. Using only the larger sizes, those above 550 nm where there is no contribution by doubly charged particles, 1.531 + 0.000i was fit. This suggests that an accurate complex refractive index could be fit to the data if enough extinction cross sections are measured in the absence of multiply-charged particles. In contrast, the complex refractive index fit to the smaller particles, diameters less than 550 nm, was 1.508 + 0.000i, represented by the dashed line in Figure 4.4. The dashed line doesn't appear to fit any of the measured extinction cross sections demonstrating the important role of larger, singly charged, particles in accurately fitting a complex refractive index.

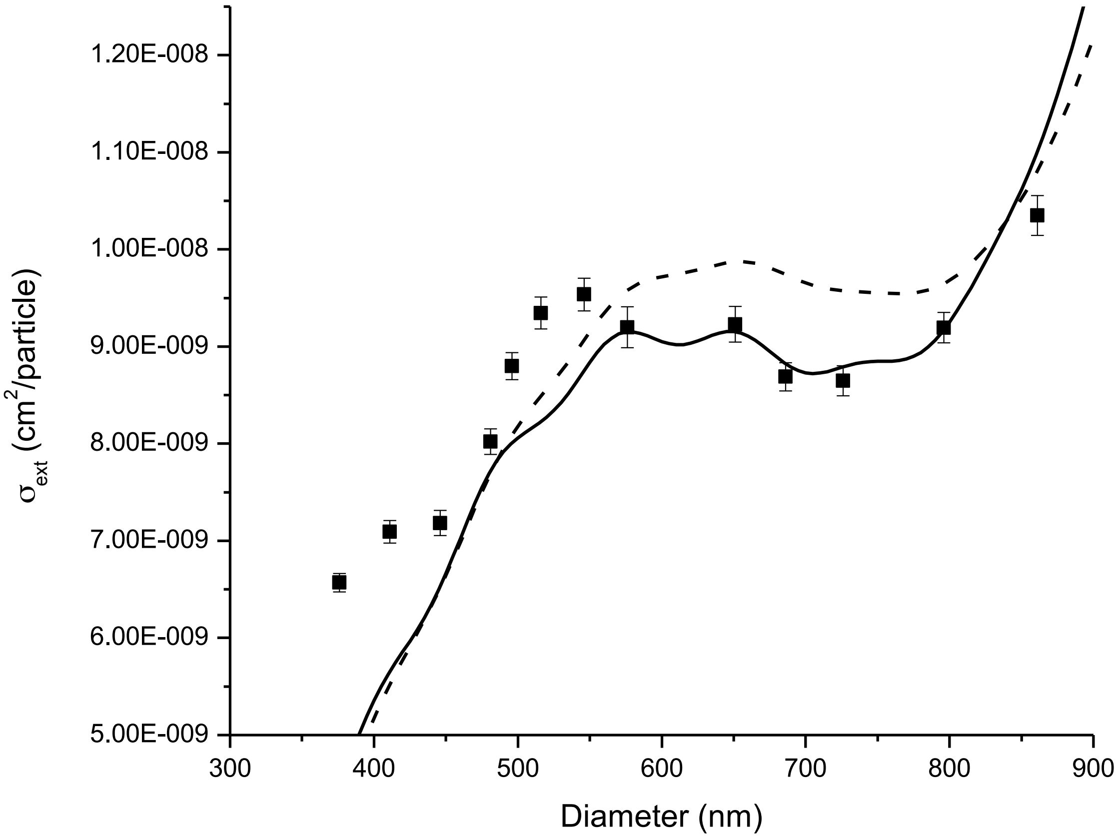

Figure 4.4 Measured squalene extinction cross sections. The solid line respresents the complex refractive index 1.530 + 0.000i, the dashed line represents the complex refractive index 1.508 + 0.000i fit to particles smaller than 550 nm.

Figure 4.5 presents the percent difference between the measured extinction cross sections and theoretical extinction cross sections predicted for the complex refractive index 1.530 + 0.000i. The vertical division at 580 nm represents the point at which doubly-charged particles begin to contribute to the measured cross sections. As the particle size decreases the contribution of doubly-charged, and in some cases triply-charged, particles become more apparent. The red lines represents an exponential decay function fit to the data, which also approached zero near 580 nm. All CRD experiments presented in this work were conducted between 600 and 900 nm where, as illustrated by

Figure 4.5, there is no contribution of multiply charged particles. Experiments presented here were conducted in the tailing region of the nebulizer output, so the concentration of double-charged particles was dropping off with size. Additionally the cut point of the inertial impactor is 915 nm. Operating in this region ensures that few large particles were generated by the nebulizer and fewer still are transmitted through the DMA. Operating in the absence of doubly- and triply-charged particles greatly improves the accuracy of extinction cross section measurements.

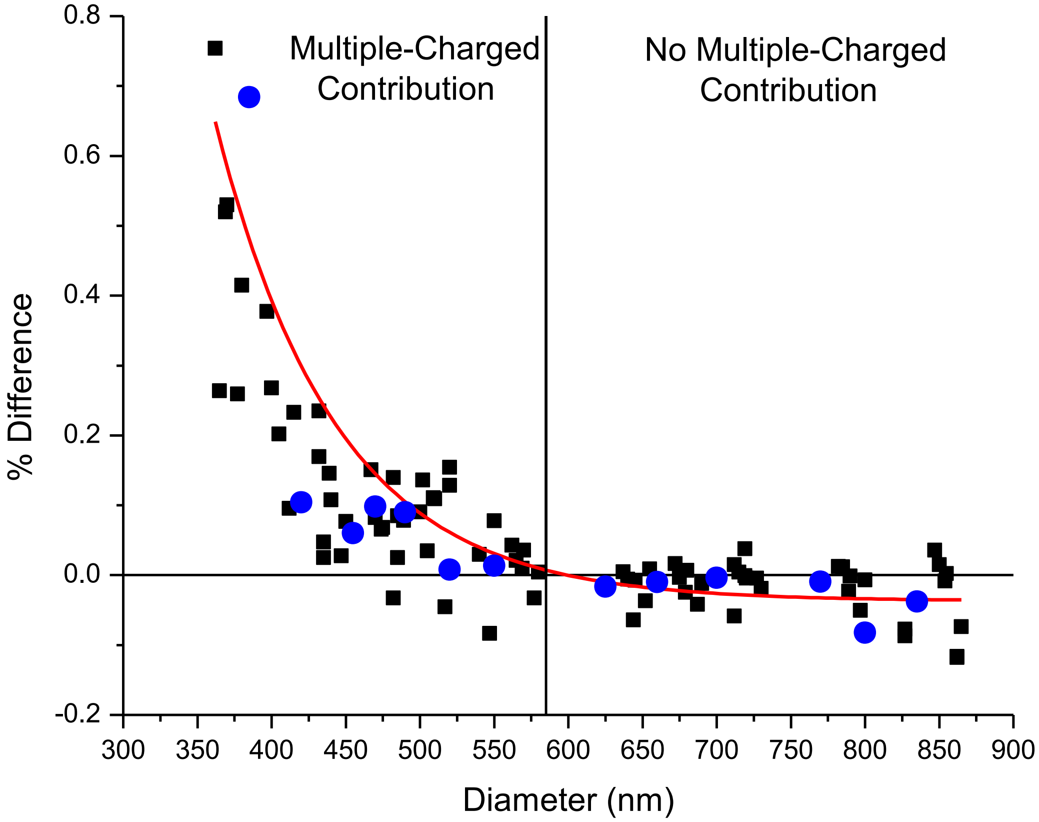

Figure 4.5 The percent difference of collected squalene extinction cross sections compared to the theoretical values predicted by Mie theory. The red line represents an exponential decay for the black square points representing the percent difference adjusted to the corresponding Δd value. The blue points represent the average percent difference at each selected particle diameter.

4.4 Conclusions

The importance of mixing state in the overall optical properties of an aerosol mixture is demonstrated in Section 4.2. Assuming an internal mixture and utilizing the volume fraction mixing rule underestimated the measured extinction cross sections at large particle sizes for the squalane:squalene external mixture. Averaging the extinction cross sections for the pure particles gave a more accurate estimate of the observed extinction but also led to a best fit complex refractive index with an absorbing component k = 0.006. Both components in this mixture are pure scatterers so while this complex refractive index more closely resembles the measured extinction cross sections it also supports the need for a secondary absorption method in order to accurately determine the complex refractive index of an external mixture.

Literature studies of external aerosol mixtures utilize a synergistic approach in order to accurately determine the complex refractive index of ambient aerosols. For example, a study by Raut et al. measured aerosol absorption using an aethalometer and used that same measurement to parameterize the inversion of collected Lidar and sunphotometer data.[63] Ebert et al. utilized total reflection X-ray fluorescence and high resolution scanning electron microscopy to calculate the complex refractive index of filter samples based on size distribution and particle composition information.[62] A cavity ring down study by Dinar et al. collected ambient aerosols on a filter an re-aerosolized the collected particles losing any mixing state information but generating uniform internally mixed particles therefore selecting the mixing state.[18]

An alternative external mixture, made up of squalene particles of multiple charge states, was presented in Section 4.3. Multiply-charged particles are an inevitable complication when utilizing a DMA for size selection. Many particles of different sizes may exhibit equal electrical mobilities based on their charge state, and as a result particles of many charge states will be transmitted through the DMA. CRDS studies in the literature utilize a correction proposed by Hasenkopf et al. in order to predict and account for doubly- or triply-charged particles within 5%.[64] Figure 4.5 demonstrates the affect doubly-charged particles have on the measured extinction cross sections at small particle sizes. However, if extinction cross sections are collected between 600 to 900 nm an accurate complex refractive index can still be determined. Not only is this the region without multiply-charged particles based on the inertial impactor it is also the region most sensitive to small differences in refractive index. Extinction cross section measurements for particles larger than 580 nm 'anchor' the complex refractive index in the fitting process.

CHAPTER 5

APPLICATIONS OF CAVITY RING DOWN SPECTROSCOPY FOR THE EXPLORATION OF PHASE REQUIRING FURTHER EXPERIMENTATION

5.1 Heated Cavity Ring Down Spectroscopy

In previous chapters CRDS was presented as a highly accurate technique for the measurement of aerosol extinction cross sections leading to accurate complex refractive indices for purely scattering and weakly absorbing aerosol particles. An accurate representation of aerosol optical properties is critical for the understanding of their role in atmosphere. More specifically, report of accurate aerosol absorption is necessary in order to predict their contribution to climate system. Many techniques have been used for the measurement of aerosol absorption, photoacoustic spectroscopy for instance has demonstrated a high level of sensitivity to weakly absorbing aerosol particles reporting absorption values as small as $k = 0.007$.[23] Here CRDS is utilized for the measurement of aerosol absorption in the absence scattering by the particle. In order to measure this absorption, particles of interest are vaporized before flowing into the CRD cell. The resulting extinction is primarily due to absorption by the vapor with a negligible contribution by Rayleigh scattering. An alternative absorption measurement of this kind could be used to validate, or even parameterize, the absorption component of the complex refractive index thereby improving the accuracy of the fitting process.

Many previous CRDS studies report erroneous absorption values for purely scattering aerosols. For instance, Pettersson et al. reported the complex refractive index of dioctyl sebacate (DOS) as 1.455 + 0.003i at 532 nm.[37] DOS, however, does not absorb in the UV-Visible region. The bulk complex refractive index measurement techniques presented in Chapter 2 yielded a complex refractive index of 1.451 + 0.000i at 532 nm. A more direct absorption measurement could be used to parameterize the complex refractive index fitting process improving the accuracy of the reported scattering component, n. In a study by Freedman et al. total particle extinction was measured using CRDS at 532nm; the complex refractive index was fit with a fixed absorption component k=0.000. In order to fit a complex refractive index, the scattering component, n, was then varied until a best-fit was determined.[30] Unfortunately, the reported values of n were larger than values measured by other groups using alternative techniques; for example the value reported for sodium fluoride was 1.351 + 0.00i[30] compared to the value of 1.326 + 0.00i reported by Bass et al.[60] This study by Freedman et al. demonstrates the need for careful aerosol extinction cross section measurements in studies were the absorption value is used to parameterize the fitting process.

Previous chapters have demonstrated the precise measurement of aerosol extinction cross sections for both weakly-absorbing and purely-scattering aerosols at 355 nm. Extinction cross section measurements of squalene particles presented in Chapter 3 were within 3% of those predicted by Mie theory. Additionally, Chapter 3 presented measurements for a binary absorbing aerosol species; the smallest absorption in this series was k = 0.004. More direct measurements of this weak absorption could be used to validate this small k value. In this section CRDS is utilized for the measurement of extinction by absorption of a vaporized mixture of an absorbing compound, 2-(2-benzotriazol-2-yl)-6-dodecyl-4-methylphenol (BDMP), and a purely scattering compound, squalane. The complex refractive index measured for this aerosolized mixture was 1.505 + 0.028i. Here BDMP : squalane aerosols are size selected, vaporized, and flowed into the CRD cell where extinction is measured.

Instrument Description

Particles were generated from a reservoir of 15% BDMP in squalane using a concentric nebulizer. These polydisperse disperse particles were then size selected using a differential mobility analyzer (DMA). The DMA output is a monodisperse particle flow that passes into the mixing region where flow stabilizing dry nitrogen is introduced. From here particles flow into the vaporizing region, an 8 inch section of glass tubing with an outer diameter of 0.5 inches heated to 300 °C. The vapor then flows into the 120 °C heated CRD cell. A condensation particle counter at the end of the heated CRD cell measured the number density of any particles in CRD cell and provided the 1.5 lpm total flow. A reported number density of 0.0 particles/cm^3, measured after the vaporizing region, validated that particles had been completely vaporized. The ring down signal is collected by a photomultiplier tube and processed using a custom LabVIEW program that reports total extinction in real time.

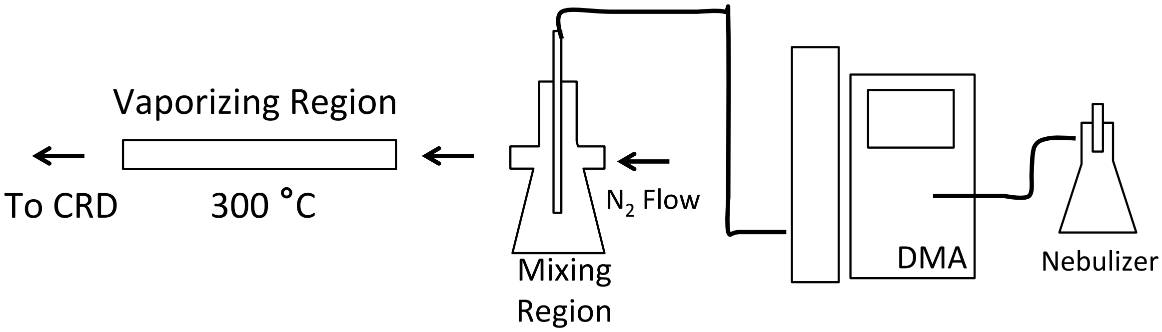

Figure 5.1 Aerosol vaporization instrumental setup.

Extinction Measurements of Vaporized Particles

In order to validate the heated CRD cell absorption measurements pure squalane particles were size selected and vaporized. Squalane does not absorb at 355 nm, meaning no extinction by absorption should be observed. The aerosol number density measured after the heated CRD cell was consistently less than 80 particles/cm^3 indicating that some vapor may have condensed over the length of the CRD cell. However, the extinction did not vary significantly from zero indicating any condensed particles were small and did not contribute appreciably to the observed extinction. This result also suggests that any extinction contributed by Rayleigh scattering was negligible. For the remainder of Section 5.1, all extinction measurements of vaporized aerosols will be referred to as absorption.

The absorbing particles vaporized in this experiment were 15% BDMP in squalane. The measured complex refractive for this mixture is 1.501 + 0.029i, reported in Chapter 3. For the five particle sizes selected and vaporized, the absorption was predicted based on the molar absorptivity and volume BDMP present in the particles prior to vaporization. Figure 5.2 compares the measured (α_{obs}) and predicted (α_{pred}) absorption for each particle diameter. In all case the absorption measured was less than half of the predicted absorption.

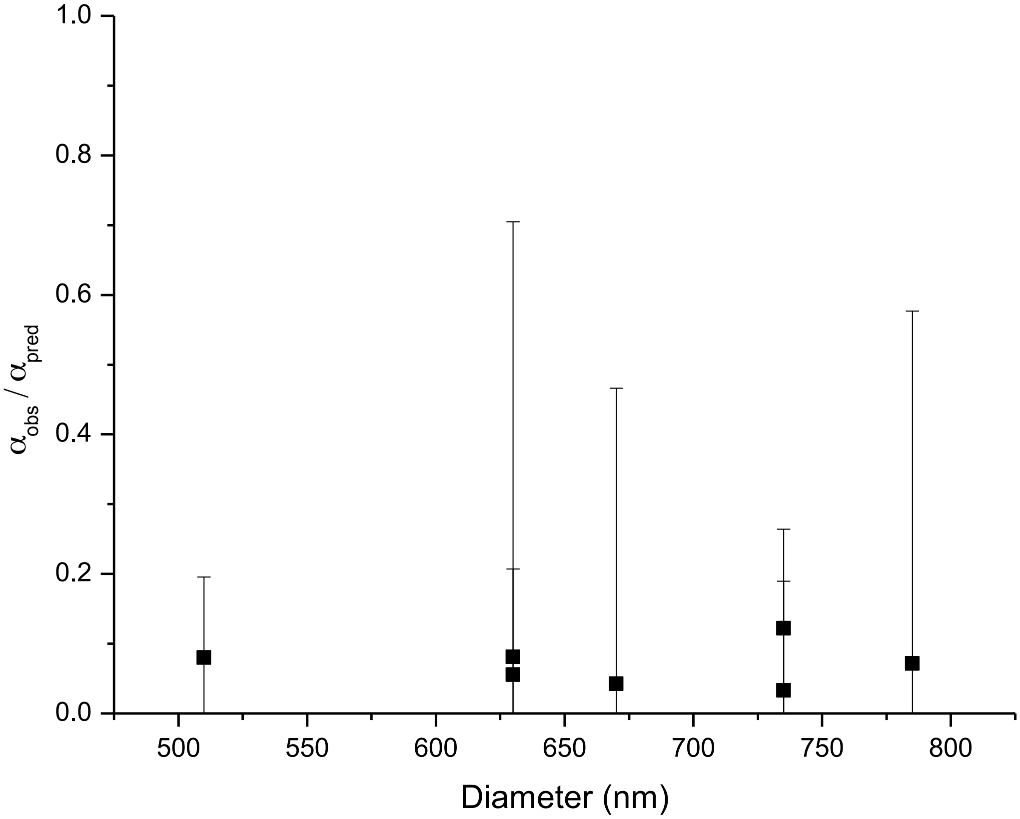

Figure 5.2 Heated cavity ring down absorption measurement of 15% BDMP : squalane vapor compared to predicted absorption. A lower bound is applied to the negative error making them artificially small based on the limited likelihood that a negative absorption would be observed.

The difference between predicted and measured absorption was not consistent between sizes or experiments. This means that the absorbing vapor was not lost to the small particles that condensed within the CRD cell. Instead, vapor was likely lost in the tubing, the vaporizing region, or the CRD cell. Temperature adjustment of the CRD cell and the vaporizing region did not yield meaningful change in the measured extinction by absorption indicating that no vapor was liberated from the walls of the vaporizer of CRD cell. Furthermore, a consistent particle number density of 80 particles/cm^3 remained. The

CRD cell was heated to 120 °C, substantially cooler than the 300 °C of the vaporizing region, this temperature gradient could promote condensation of vapor on the walls of the CRD cell. Unfortunately, we were not able to increase the temperature of the CRD cell past 120 °C based on concerns for the highly-reflective mirrors.

The reduced absorption cannot be explained by particle formation, either. No particles were detected directly after the vaporizing region, and once vapor travelled through the ring down cell a particle concentration of less than or equal to 80 particles/cm^3 was found. Tests with vaporized squalane particles also exhibit particle generation over the length of the CRD cell. However, these particles did not produce an appreciable change in ring down signal meaning that they are likely small and cannot account for the loss of BDMP. Further investigation into the fate of the absorbing vapor is needed.

5.2 Supercooled and Frozen Aerosol Particles

Many ambient sampling studies have reported collection of supercooled and frozen particles in the atmosphere.[65] Other studies have reported the collection of frozen particles in the stratosphere[65,66] while some suggest that aerosol particles may form glasses.[67,68] Supercooled particles are particles that have cooled past their melting point without crystalizing. Many studies have examined the impact of supercooling or freezing on organic aerosol rate of reaction as well as their impact on cloud nucleation.[69-71] Much of the challenge in working with supercooled and frozen aerosol particles lies in identification of phase. Renbaum et al. used the relative rate of reaction to identify supercooled versus frozen particles reporting that the supercooled particles reacted more quickly than frozen particles.[70] Yamato et al. identified frozen stratospheric particles by comparing collected ambient aerosols to lab-generated frozen particles.[65]

There are few nondestructive methods for differentiation of particle phase. This section begins to examine the role of phase in aerosol optical properties in order to introduce CRDS as a nondestructive, *in situ*, measurement technique that could be utilized for the determination of particle phase. Initial nephelometer measurements collected by Renbaum showed that supercooled particles were 23% less effective at scattering UV radiation than frozen particles.[72] The goal of this section is to reproduce this measurement utilizing CRDS for the measurement of phase-dependent optical properties for several monounsaturated carboxylic acids. This information would not only serve as an *in situ* particle phase identifier but would also yield important information about the role of phase in the aerosol direct effect.

Instrument Description

A 0.901 lpm dry nitrogen flow is passed over a reservoir of the selected compound heated to 143 °C. In this case brassidic and elaidic acid were used. The vapor then travels through a 256 °C condensation region before entering a cold trap. The cold trap was submerged in a dry ice isopropanol bath, -70 °C, and particles traveling through this region were frozen. Particle that bypassed the cooling region approached room temperature and based on previous work from our group[70,73,74] were assumed to have supercooled. From this point particles that have bypassed the cold trap will be referred to as liquid-like due to lack of verification that they have supercooled. A scanning mobility particle sizer (SMPS) indicated no difference in geometric mean or standard deviation between particle ensembles traveling through or bypassing the cooling region suggesting particles were frozen in a spherical shape.

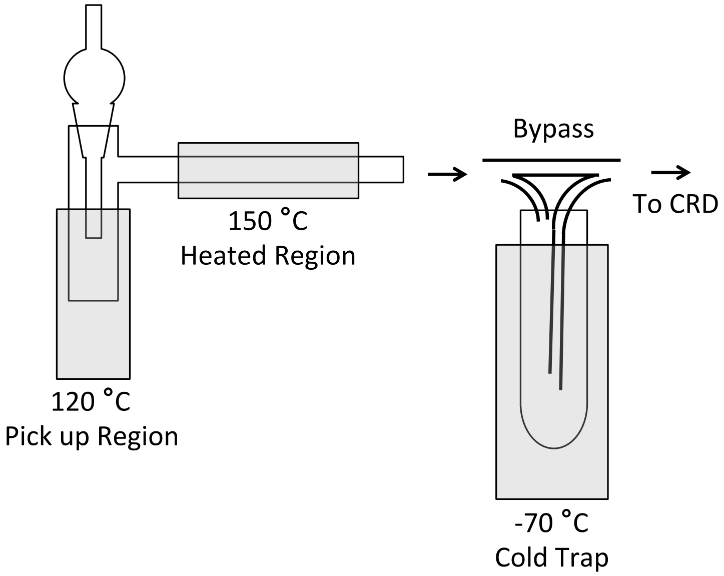

Figure 5.3 Diagram of the homogeneous nucleation region used in the generation of supercooled and frozen aerosol particles.

Extinction Measurements

The extinction measurements for liquid-like and frozen aerosol particles are displayed in Table 5.1 as mass scattering coefficients (μ_{scat}) along with the ratio of these values. The values displayed represent the average extinction over an 8 – 12 minute measurement divided by the total mass concentration of the particle distribution. These averages display extreme variability due to instability in the particle source. The particle distribution was collected by an SMPS and was characterized by the geometric mean and standard deviation. The geometric mean would gradually increase by as much 200 nm from the beginning to the end of the day, approximately 8 hours. This change is particularly noteworthy considering a typical initial geometric mean is near 140 nm increasing to nearly 365 nm. Additionally, the particle concentrations measured by the

CPC after the CRD cell varied greatly over the course of one 8 – 12 minute measurement. These swings in concentration and particle distribution likely account for the large deviations associated with the mass scattering coefficients reported in Table 5.1.

Table 5.1 Comparison of mass scattering coefficients of liquid-like ($\mu_{Scat,LL}$) and frozen ($\mu_{Scat,FR}$) aerosol particles as measured by cavity ring down spectroscopy. *Measurement recorded by Renbaum using a nephelometer[72]

	Liquid-Like (m^2/g) $\mu_{scat,LL}$	Frozen (m^2/g) $\mu_{scat,FR}$	$\mu_{scat,LL}/\mu_{scat,FR}$
Brassidic Acid	2.3* 0.23	3.0* 0.07	0.77* 3.27 ± 0.028
Elaidic Acid	4.01	1.91	2.09 ± 0.038
	0.008	0.004	1.98 ± 0.475
	0.28	0.12	2.36 ± 0.166
	1.05	0.94	1.12 ± 0.017
	6.93	3.72	1.86 ± 0.405

Measurements recorded by Renbaum using a nephelometer are presented in Table 5.1 and indicated that supercooled brassidic acid particles have a mass scattering coefficient of 2.3 compared to 3.0 associated with frozen particles;[72] indicating that frozen particles scatter light more efficiently than supercooled particles of equal size and composition. Brassidic and elaidic acid measurements recorded by CRDS did not agree with these values. Despite the wide range associated with the CRDS measurement the reported values suggest that liquid particles scatter light more efficiently than frozen particles. One explanation for this difference in scattering efficiency could be attributed to the rate of the cooling in the liquid-like, i.e. assumed supercooled particles. If particle cooled too rapidly seed crystals, or so-called "domains", could form within the particle generating more surfaces for refraction increasing the scattering efficiency of the particle.[75,76]

The assumed phase of the measured particles is an additional factor inhibiting meaningful conclusions. Renbaum utilized the observed phase-dependent rate of reaction to differentiate phases.[72] To this point the phase of the particles has been assumed based on their transit through or around the cold trap. There remains a need for a nondestructive, and ideally *in situ*, technique for the validation of aerosol phase. Additional work to stabilize the particle source and narrow the distribution is necessary before further measurements can be collected.

References

(1) Seinfeld, J. H.; Pandis, S. N. *Atmospheric Chemistry and Physics*; John Wiley & Sons, 2012.

(2) Kanakidou, M.; Seinfeld, J. H.; Pandis, S. N.; Barnes, I.; Dentener, F. J.; Facchini, M. C.; Dingenen, R. V.; Ervens, B.; Nenes, A.; Nielsen, C. J. *Atmospheric Chemistry and Physics* **2005**, *5*, 1053–1123.

(3) Finlayson-Pitts, B. J.; James N Pitts, J. *Chemistry of the Upper and Lower Atmosphere*; Academic Press, 1999.

(4) Jimenez, J. L.; Canagaratna, M. R.; Donahue, N. M.; Prevot, A. S. H.; Zhang, Q.; Kroll, J. H.; DeCarlo, P. F.; Allan, J. D.; Coe, H.; Ng, N. L.; Aiken, A. C.; Docherty, K. S.; Ulbrich, I. M.; Grieshop, A. P.; Robinson, A. L.; Duplissy, J.; Smith, J. D.; Wilson, K. R.; Lanz, V. A.; Hueglin, C.; Sun, Y. L.; Tian, J.; Laaksonen, A.; Raatikainen, T.; Rautiainen, J.; Vaattovaara, P.; Ehn, M.; Kulmala, M.; Tomlinson, J. M.; Collins, D. R.; Cubison, M. J.; Dunlea, E. J.; Huffman, J. A.; Onasch, T. B.; Alfarra, M. R.; Williams, P. I.; Bower, K.; Kondo, Y.; Schneider, J.; Drewnick, F.; Borrmann, S.; Weimer, S.; Demerjian, K.; Salcedo, D.; Cottrell, L.; Griffin, R.; Takami, A.; Miyoshi, T.; Hatakeyama, S.; Shimono, A.; Sun, J. Y.; Zhang, Y. M.; Dzepina, K.; Kimmel, J. R.; Sueper, D.; Jayne, J. T.; Herndon, S. C.; Trimborn, A. M.; Williams, L. R.; Wood, E. C.; Middlebrook, A. M.; Kolb, C. E.; Baltensperger, U.; Worsnop, D. R. *Science* **2009**, *326*, 1525–1529.

(5) Paeth, H.; Feichter, J. *Climate dynamics* **2006**.

(6) Martineau, R. J.; Novello, D. P. *The Clean Air Act Handbook*; American Bar Association, 2004.

(7) Stocker, T. F.; Qin, D.; Plattner, G. K.; Tignor, M.; Allen, S. K.; Boschung, J.; Nauels, A.; Xia, Y.; Bex, V; Midgley, P. M. *IPCC, 2013: Climate Cange 2013: The Physcial Basis. Contribution of Working Group 1 to the Fifth Assessment Report of the Intergovernmental Panel on Climate Change*; Cambridge University Press: Cambridge, United Kingdom and New York, NY USA, 2013; p. 1535.

(8) Toole, J. R.; Renbaum-Wolff, L.; Smith, G. D. *Aerosol Science and Technology* **2013**, *47*, 955–965.

(9) Moosmüller, H.; Chakrabarty, R. K.; Arnott, W. P. *Journal of Quantitative Spectroscopy and Radiative Transfer* **2009**, *110*, 844–878.

(10) Andreae, M. O.; Gelencsér, A. *Atmospheric Chemistry and Physics* **2006**, *6*, 3131–3148.

(11) Charlson, R. J.; Schwartz, S. E.; Hales, J. M.; Cess, R. D.; Coakley, J. A.; Hansen, J. E.; Hofmann, D. J. *Science* **1992**, *255*, 423–430.

(12) Bohren, C. F.; Huffman, D. R. *Absorption and Scattering of Light by Small Particles*; John Wiley & Sons, 2008.

(13) Lohmann, U.; Feichter, J. *Atmospheric Chemistry and Physics* **2005**, *5*, 715–737.

(14) Menon, S.; Del Genio, A. D.; Koch, D.; Tselioudis, G. *http://dx.doi.org/10.1175/1520-0469(2002)059<0692:GSOTAI>2.0.CO;2* **2002**.

(15) Haywood, J.; Boucher, O. *Rev. Geophys.* **2000**, *38*, 513.

(16) Raut, J. C.; Chazette, P. *Atmospheric Chemistry and Physics* **2008**, *8*, 901–919.

(17) Raut, J. C.; Chazette, P. *Atmospheric Chemistry and Physics* **2007**, *7*, 2797–2815.

(18) Dinar, E.; Riziq, A. A.; Spindler, C.; Erlick, C.; Kiss, G.; Rudich, Y. *Faraday Discuss.* **2008**, *137*, 279–95–discussion297–318.

(19) Lack, D. A.; Lovejoy, E. R.; Baynard, T.; Pettersson, A.; Ravishankara, A. R. *Aerosol Science and Technology* **2006**, *40*, 697–708.

(20) Ma, L.; Thompson, J. E. *Anal. Chem.* **2012**, *84*, 5611–5617.

(21) Washenfelder, R. A.; Flores, J. M.; Brock, C. A.; Brown, S. S.; Rudich, Y. *Atmospheric Measurement Techniques Discussions* **2013**, *6*, 113–157.

(22) Lack, D. A.; Cappa, C. D. *Atmospheric Chemistry and Physics* **2010**, *10*, 4207–4220.

(23) Lack, D. A.; Langridge, J. M.; Bahreini, R.; Cappa, C. D.; Middlebrook, A. M.; Schwarz, J. P. *Proceedings of the National Academy of Sciences* **2012**, *109*, 14802–14807.

(24) Slowik, J. G.; Cross, E. S.; Han, J.-H.; Davidovits, P.; Onasch, T. B.; Jayne, J. T.; Williams, L. R.; Canagaratna, M. R.; Worsnop, D. R.; Chakrabarty, R. K.; Moosmüller, H.; Arnott, W. P.; Schwarz, J. P.; Gao, R.-S.; Fahey, D. W.; Kok, G. L.; Petzold, A. *Aerosol Science and Technology* **2007**, *41*, 295–314.

(25) Tombette, M.; Chazette, P.; Sportisse, B.; Roustan, Y. *Atmospheric Chemistry and Physics* **2008**, *8*, 7115–7132.

(26) Berden, G.; Peeters, R.; Meijer, G. *International Reviews in Physical Chemistry* **2000**, *19*, 565–607.

(27) Busch, K. W.; Busch, M. A. *Cavity-ringdown Spectroscopy*; Amer Chemical Society, 1999.

(28) Riziq, A. A.; Erlick, C.; Dinar, E.; Rudich, Y. *Atmospheric Chemistry and Physics Discussions* **2006**, *6*, 12347–12387.

(29) Lang-Yona, N.; Rudich, Y.; Segre, E.; Dinar, E.; Abo Riziq, A. *Anal. Chem.* **2009**, *81*, 1762–1769.

(30) Freedman, M. A.; Hasenkopf, C. A.; Beaver, M. R.; Tolbert, M. A. *J Phys Chem A* **2009**, *113*, 13584–13592.

(31) Mason, B. J.; King, S.-J.; Miles, R. E. H.; Manfred, K. M.; Rickards, A. M. J.; Kim, J.; Reid, J. P.; Orr-Ewing, A. J. *J Phys Chem A* **2012**, *116*, 8547–8556.

(32) Du, K.; Wang, Y.; Chen, B.; Wang, K.; Chen, J.; Zhang, F. *Atmospheric Environment* **2011**, *45*, 7113–7120.

(33) Mishchenko, M. I. *Journal of Quantitative Spectroscopy and Radiative Transfer* **2009**, *110*, 1210–1222.

(34) Abo Riziq, A.; Erlick, C.; Dinar, E.; Rudich, Y. *Atmospheric Chemistry and Physics* **2007**, *7*, 1523–1536.

(35) Spindler, C.; Riziq, A. A.; Rudich, Y. *Aerosol Science and Technology* **2007**, *41*, 1011–1017.

(36) Rudich, Y.; RIZIQ, A.; Erlick, C.; Adler, G. *Geochimica et …* **2009**.

(37) Pettersson, A.; Lovejoy, E. R.; Brock, C. A.; Brown, S. S.; Ravishankara, A. R. *Journal of Aerosol Science* **2004**, *35*, 995–1011.

(38) Zarzana, K. J.; De Haan, D. O.; Freedman, M. A.; Hasenkopf, C. A.; Tolbert, M. A. *Environ. Sci. Technol.* **2012**, *46*, 4845–4851.

(39) Abo Riziq, A.; Trainic, M.; Erlick, C.; Segre, E.; Rudich, Y. *Atmospheric Chemistry and Physics* **2008**, *8*, 1823–1833.

(40) Pant, A. *Geophys. Res. Lett.* **2004**, *31*, L12111.

(41) Thompson, J. E.; Barta, N.; Policarpio, D.; DuVall, R. *Opt. Express* **2008**, *16*, 2191.

(42) Baynard, T.; Lovejoy, E. R.; Pettersson, A.; Brown, S. S.; Lack, D.; Osthoff, H.; Massoli, P.; Ciciora, S.; Dube, W. P.; Ravishankara, A. R. *Aerosol Science and Technology* **2007**, *41*, 447–462.

(43) Miles, R. E. H.; Rudić, S.; Orr-Ewing, A. J.; Reid, J. P. *J Phys Chem A* **2010**, *114*, 7077–7084.

(44) Berden, G.; Engeln, R. *Cavity ring-down spectroscopy: techniques and applications*; 2009.

(45) Atkinson, D. B. *Analyst* **2003**, *128*, 117–125.

(46) van de Hulst, H. C. *Light Scattering by Small Particles*; Courier Dover Publications, 2012.

(47) Flagan, R. C. *Aerosol Science and Technology* **1999**, *30*, 556–570.

(48) Collins, A. M.; Dick, W. D.; Romay, F. J. *Aerosol Science and Technology* **2013**, *47*, 177–182.

(49) Painter, L. R.; Attrey, J. S.; Hubbell, H. H.; Birkhoff, R. D. *J. Appl. Phys.* **1984**, *55*, 756.

(50) Kozma, I. Z.; Krok, P.; Riedle, E. *J. Opt. Soc. Am. B, JOSAB* **2005**, *22*, 1479–1485.

(51) Ghazi, R.; Olfert, J. S. *Aerosol Science and Technology* **2013**, *47*, 192–200.

(52) Rheims, J.; Köser, J.; Wriedt, T. *Measurement Science and Technology* **1997**, *8*, 601.

(53) Fujiwara, H. *Spectroscopic Ellipsometry*; John Wiley & Sons, 2007.

(54) Tompkins, H. G.; McGahan, W. A. *Spectroscopic Ellipsometry and Reflectometry*; Wiley-Interscience, 1999.

(55) Lang-Yona, N.; Abo-Riziq, A.; Erlick, C.; Segre, E.; Trainic, M.; Rudich, Y. *Phys. Chem. Chem. Phys.* **2009**, *12*, 21.

(56) Erlick, C.; Abbatt, J. P. D.; Rudich, Y. *J. Atmos. Sci.* **2011**, *68*, 1845–1852.

(57) Garvey, D. M.; Pinnick, R. G. *Aerosol Science and Technology* **1983**, *2*, 477–488.

(58) Kirchstetter, T. W. *J. Geophys. Res.* **2004**, *109*, D21208.

(59) Hearn, J. D.; Lovett, A. J.; Smith, G. D. *Phys. Chem. Chem. Phys.* **2005**, *7*, 501–511.

(60) Bass, M.; DeCusatis, C.; Enoch, J.; Lakshminarayanan, V.; Li, G.; MacDonald, C.; Mahajan, V.; Van Stryland, E. *Handbook of Optics, Third Edition Volume IV: Optical Properties of Materials, Nonlinear Optics, Quantum Optics (set)*; McGraw Hill Professional, 2009.

(61) Khalizov, A. F.; Xue, H.; Wang, L.; Zheng, J.; Zhang, R. *J Phys Chem A* **2009**, *113*, 1066–1074.

(62) Ebert, M.; Weinbruch, S.; Hoffmann, P.; Ortner, H. M. *Atmospheric Environment* **2004**, *38*, 6531–6545.

(63) Raut, J. C.; Chazette, P.; Fortain, A. *Atmospheric Environment* **2009**, *43*, 860–868.

(64) Hasenkopf, C. A.; Beaver, M. R.; Trainer, M. G.; Langley Dewitt, H.; Freedman, M. A.; Toon, O. B.; McKay, C. P.; Tolbert, M. A. *Icarus* **2010**, *207*, 903–913.

(65) Yamato, M.; Ono, A. *Meteorological Society of Japan Journal* **1989**, *67*, 147–166.

(66) Yun, Y.; Penner, J. E. *J. Geophys. Res.* **2012**, *117*, n/a–n/a.

(67) Koop, T.; Bookhold, J.; Shiraiwa, M.; Pöschl, U. *Phys. Chem. Chem. Phys.* **2011**, *13*, 19238–19255.

(68) Zobrist, B.; Marcolli, C.; Pedernera, D. A.; Koop, T. *Atmospheric Chemistry and Physics Discussions* **2008**, *8*, 9263–9321.

(69) Sassen, K.; Dodd, G. C. *J. Atmos. Sci.* **1988**, *45*, 1357–1369.

(70) Renbaum, L. H.; Smith, G. D. *Phys. Chem. Chem. Phys.* **2009**, *11*, 2441.

(71) Arakawa, M.; Yamashita, Y.; Funatsu, K. *Phys. Chem. Chem. Phys.* **2005**, *25*, 10–19.

(72) Renbaum, L. H. Kinetics, Products, and Optical Property Chenges During the Heterogeneous Oxidation of Organic Aerosols, University of Georgia, 2011, pp. 1–221.

(73) Hearn, J. D.; Smith, G. D. *Geophys. Res. Lett.* **2006**, *33*, L17805.

(74) Renbaum, L. H.; Smith, G. D. *Atmospheric …* **2011**.

(75) Pruppacher, H. R. *J. Atmos. Sci.* **1995**, *52*, 1924–1933.

(76) Zhao, X.; Kivelson, D. *The Journal of Physical Chemistry* **1995**, *99*, 6721–6732.